Baglivo I, Esposito S, De Cesare L, Sparago A, Anvar Z, Riso V, Cammisa M, Fattorusso R, Grimaldi G, Riccio A, et al. 2013. Genetic and epigenetic mutations affect the DNA binding capability of human ZFP57 in transient neonatal diabetes type 1. *FEBS Lett* **587:** 1474–1481.
Barbaux S, Gascoin-Lachambre G, Buffat C, Monnier P, Mondon F, Tonanny MB, Pinard A, Auer J, Bessières B, Barlier A, et al. 2012. A genome-wide approach reveals novel imprinted genes expressed in the human placenta. *Epigenetics* **7:** 1079–1090.
Bourc'his D, Xu GL, Lin CS, Bollman B, Bestor TH. 2001. Dnmt3L and the establishment of maternal genomic imprints. *Science* **294:** 2536–2539.
Buiting K. 2010. Prader-Willi syndrome and Angelman syndrome. *Am J Med Genet C Semin Med Genet* **154C:** 365–376.
Choufani S, Shuman C, Weksberg R. 2010. Beckwith-Wiedemann syndrome. *Am J Med Genet C Semin Med Genet* **154C:** 343–354.
Ciccone DN, Su H, Hevi S, Gay F, Lei H, Bajko J, Xu G, Li E, Chen T. 2009. KDM1B is a histone H3K4 demethylase required to establish maternal genomic imprints. *Nature* **461:** 415–418.
Constância M, Kelsey G, Reik W. 2004. Resourceful imprinting. *Nature* **432:** 53–57.
Coombes C, Arnaud P, Gordon E, Dean W, Coar EA, Williamson CM, Feil R, Peters J, Kelsey G. 2003. Epigenetic properties and identification of an imprint mark in the Nesp-Gnasxl domain of the mouse *Gnas* imprinted locus. *Mol Cell Biol* **23:** 5475–5488.
Cooper WN, Constância M. 2010. How genome-wide approaches can be used to unravel the remaining secrets of the imprintome. *Brief Funct Genomics* **9:** 315–328.
Das R, Lee YK, Strogantsev R, Jin S, Lim YC, Ng PY, Lin XM, Chng K, Yeo GSh, Ferguson-Smith AC, et al. 2013. DNMT1 and AIM1 imprinting in human placenta revealed through a genome-wide screen for allele-specific DNA methylation. *BMC Genomics* **14:** 685.
Dhayalan A, Rajavelu A, Rathert P, Tamas R, Jurkowska RZ, Ragozin S, Jeltsch A. 2010. The Dnmt3a PWWP domain reads histone 3 lysine 36 trimethylation and guides DNA methylation. *J Biol Chem* **285:** 26114–26120.
Eggermann T. 2010. Russell-Silver syndrome. *Am J Med Genet C Semin Med Genet* **154C:** 355–364.
Ehrlich M, Gama-Sosa MA, Huang LH, Midgett RM, Kuo KC, McCune RA, Gehrke C. 1982. Amount and distribution of 5-methylcytosine in human DNA from different types of tissues of cells. *Nucleic Acids Res* **10:** 2709–2721.
El-Maarri O, Buiting K, Peery EG, Kroisel PM, Balaban B, Wagner K, Urman B, Heyd J, Lich C, Brannan CI, et al. 2001. Maternal methylation imprints on human chromosome 15 are established during or after fertilization. *Nat Genet* **27:** 41–44.
Fuke C, Shimabukuro M, Petronis A, Sugimoto J, Oda T, Miura K, Miyazaki T, Ogura C, Okazaki Y, Jinno Y. 2004. Age related changes in 5-methylcytosine content in human peripheral leukocytes and placentas: An HPLC-based study. *Ann Hum Genet* **68:** 196–204.
Geuns E, De Temmerman N, Hilven P, Van Steirteghem A, Liebaers I, De Rycke M. 2007. Methylation analysis of the intergenic differentially methylated region of DLK1-GTL2 in human. *Eur J Hum Genet* **15:** 352–361.
Gregg C, Zhang J, Weissbourd B, Luo S, Schroth GP, Haig D, Dulac C. 2010. High-resolution analysis of parent-of-origin allelic expression in the mouse brain. *Science* **329:** 643–648.
Hammoud SS, Nix DA, Zhang H, Purwar J, Carrell DT, Cairns BR. 2009. Distinctive chromatin in human sperm packages genes for embryo development. *Nature* **460:** 473–478.
Harness JV, Turovets NA, Seiler MJ, Nistor G, Altun G, Agapova LS, Ferguson D, Laurent LC, Loring JF, Keirstead HS. 2011. Equivalence of conventionally-derived and parthenote-derived human embryonic stem cells. *PLoS ONE* **6:** e14499.
Hata K, Okano M, Lei H, Li E. 2002. Dnmt3L cooperates with the Dnmt3 family of de novo DNA methyltransferases to establish maternal imprints in mice. *Development* **129:** 1983–1993.
Hayashizaki Y, Shibata H, Hirotsune S, Sugino H, Okazaki Y, Sasaki N, Hirose K, Imoto H, Okuizumi H, Muramatsu M, et al. 1994. Identification of an imprinted U2af binding protein related sequence on mouse chromosome 11 using the RLGS method. *Nat Genet* **6:** 33–40.
Heyn H, Li N, Ferreira HJ, Moran S, Pisano DG, Gomez A, Diez J, Sanchez-Mut JV, Setien F, Carmona FJ, et al. 2012. Distinct DNA methylomes of newborns and centenarians. *Proc Natl Acad Sci* **109:** 10522–10527.
Hiura H, Sugawara A, Ogawa H, John RM, Miyauchi N, Miyanari Y, Horiike T, Li Y, Yaegashi N, Sasaki H, et al. 2010. A tripartite paternally methylated region within the *Gpr1-Zdbf2* imprinted domain on mouse chromosome 1 identified by meDIP-on-chip. *Nucleic Acids Res* **38:** 4929–4945.
Kanber D, Berulava T, Ammerpohl O, Mitter D, Richter J, Siebert R, Horsthemke B, Lohman D, Buiting K. 2009. The human retinoblastoma gene is imprinted. *PLoS Genet* **12:** e1000790.
Iglesias-Platas I, Court F, Camprubi C, Sparago A, Guillaumet-Adkins A, Martin-Trujillo A, Riccio A, Moore GE, Monk D. 2013. Imprinting at the *PLAGL1* domain is contained within a 70-kb CTCF/cohesin-mediated non-allelic chromatin loop. *Nucleic Acids Res* **41:** 2171–2179.
Kagami M, Sekita Y, Nishimura G, Irie M, Kato F, Okada M, Yamamori S, Kishimoto H, Nakayama M, Tanaka Y, et al. 2008. Deletions and epimutations affecting the human 14q32.2 imprinted region in individuals with paternal and maternal upd(14)-like phenotypes. *Nat Genet* **40:** 237–242.
Kagami M, O'Sullivan MJ, Green AJ, Watabe Y, Arisaka O, Masawa N, Matsuoka K, Fukami M, Matsubara K, Kato F, et al. 2010. The IG-DMR and the *MEG3*-DMR at human chromosome 14q32.2: Hierarchical interaction and distinct functional properties as imprinting control centers. *PLoS Genet* **6:** e1000992.
Kelsey G. 2010. Imprinting on chromosome 20: Tissue-specific imprinting and imprinting mutations in the GNAS locus. *Am J Med Genet C Semin Med Genet* **154C:** 377–386.
Kelsey G, Bodle D, Miller HJ, Beechey CV, Coombes C, Peters J, Williamson CM. 1999. Identification of imprinted loci by methylation-sensitive representational difference analysis: Application to mouse distal chromosome 2. *Genomics* **62:** 129–138.
Kobayashi H, Sakurai T, Imai M, Takahashi N, Fukuda A, Yayoi O, Sato S, Nakabayashi K, Hata K, Sotomaru Y, et al. 2012. Contribution of intragenic DNA methylation in mouse gametic DNA methylomes to establish oocyte-specific heritable marks. *PLoS Genet* **8:** e1002440.
Kobayashi H, Yanagisawa E, Sakashita A, Sugawara N, Kumakura S, Ogawa H, Akutsu H, Hata K, Nakabayashi K, Kono T. 2013. Epigenetic and transcriptional features of the novel human imprinted lncRNA *GPR1AS* suggest it is a functional ortholog to mouse *Zdbf2linc*. *Epigenetics* **8:** 635–645.
Kong A, Steinthorsdottir V, Masson G, Thorleifsson G, Sulem P, Besenbacher S, Jonasdottir A, Sigurdsson A, Kristinsson KT, Jonasdottir A, et al. 2009. Parental origin of sequence variants associated with complex diseases. *Nature* **462:** 868–874.
Lapunzina P, Monk D. 2011. The consequences of uniparental disomy and copy number neutral loss-of-heterozygosity during human development and cancer. *Biol Cell* **103:** 303–317.
Li X, Ito M, Zhou F, Youngson N, Zuo X, Leder P, Ferguson-Smith AC. 2008. A maternal-zygotic effect gene, *Zfp57*, maintains both maternal and paternal imprints. *Dev Cell* **15:** 547–557.
Lister R, Pelizzola M, Dowen RH, Hawkins RD, Hon G, Tonti-Filippini J, Nery JR, Lee L, Ye Z, Ngo QM, et al. 2009. Human DNA methylomes at base resolution show widespread epigenomic differences. *Nature* **462:** 315–322.
Lopes S, Lewis A, Hajkova P, Dean W, Oswald J, Forné T, Murrell A, Constância M, Bartolomei M, Walter J, et al. 2003. Epigenetic modifications in an imprinting cluster are controlled by a hierarchy of DMRs suggesting long-range chromatin interactions. *Hum Mol Genet* **12:** 295–305.
Mackay DJ, Temple IK. 2010. Transient neonatal diabetes mellitus type 1. *Am J Med Genet C Semin Med Genet* **154C:** 335–342.
Mai Q, Yu Y, Li T, Wang L, Chen MJ, Huang SZ, Zhou C, Zhou Q. 2007. Derivation of human embryonic stem cell lines from parthenogenetic blastocysts. *Cell Res* **17:** 1008–1012.
Molaro A, Hodges E, Fang F, Song Q, McCombie WR, Hannon GJ, Smith AD. 2011. Sperm methylation profiles reveal features of epigenetic inheritance and evolution in primates. *Cell* **146:** 1029–1041.
Monk D. 2010. Deciphering the cancer imprintome. *Brief Funct Genomics* **9:** 329–339.
Monk D, Arnaud P, Apostolidou S, Hills FA, Kelsey G, Stanier P, Feil R, Moore GE. 2006. Limited evolutionary conservation of imprinting in the human placenta. *Proc Natl Acad Sci* **103:** 6623–6628.
Nakabayashi K, Trujillo AM, Tayama C, Camprubi C, Yoshida W, Lapunzina P, Sanchez A, Soejima H, Aburatani H, Nagae G, et al. 2011. Methylation screening of reciprocal genome-wide UPDs identifies novel human-specific imprinted genes. *Hum Mol Genet* **20:** 3188–3197.
Nakamura T, Arai Y, Umehara H, Masuhara M, Kimura T, Taniguchi H, Sekimoto T, Ikawa M, Yoneda Y, Okabe M. 2007. PGC7/Stella protects against DNA demethylation in early embryogenesis. *Nat Cell Biol* **9:** 64–71.
Noguer-Dance M, Abu-Amero S, Al-Khtib M, Lefèvre A, Coullin P, Moore GE, Cavaillé J. 2010. The primate-specific microRNA gene cluster (C19MC) is imprinted in the placenta. *Hum Mol Genet* **19:** 3566–3582.
Okae H, Hiura H, Nishida Y, Funayama R, Tanaka S, Chiba H, Yaegashi N, Nakayama K, Sasaki H, Arima T. 2011. Re-investigation and RNA sequencing-based identification of genes with placenta-specific imprinted expression. *Hum Mol Genet* **21:** 548–558.
Park KY, Sellars EA, Grinberg A, Huang SP, Pfeifer K. 2004. The H19 differentially methylated region marks the parental origin of a heterologous locus without gametic DNA methylation. *Mol Cell Biol* **24:** 3588–3595.
Proudhon C, Duffié R, Ajjan S, Cowley M, Iranzo J, Carbajosa G, Saadeh H, Holland ML, Oakey RJ, Rakyan VK, et al. 2012. Protection against de

novo methylation is instrumental in maintaining parent-of-origin methylation inherited from the gametes. *Mol Cell* **47:** 909–920.
Quenneville S, Verde G, Corsinotti A, Kapopoulou A, Jakobsson J, Offner S, Baglivo I, Pedone PV, Grimaldi G, Riccio A, et al. 2011. In embryonic stem cells, ZFP57/KAP1 recognize a methylated hexanucleotide to affect chromatin and DNA methylation of imprinting control regions. *Mol Cell* **44:** 361–372.
Ramowitz LK, Bartolomei MS. 2011. Genomic imprinting: Recognition and marking of imprinted loci. *Curr Opin Genet Dev* **22:** 72–78.
Romanelli V, Nevado J, Fraga M, Trujillo AM, Mori MÁ, Fernández L, Pérez de Nanclares G, Martínez-Glez V, Pita G, Meneses H, et al. 2011. Constitutional mosaic genome-wide uniparental disomy due to diploidisation: An unusual cancer-predisposing mechanism. *J Med Genet* **48:** 212–216.
Schroeder DI, Blair JD, Lott P, Yu HO, Hong D, Crary F, Ashwood P, Walker C, Korf I, Robinson WP, et al. 2013. The human placenta methylome. *Proc Natl Acad Sci* **110:** 6037–6042.
Sharp A, Migliavacca E, Dupre Y, Stathaki E, Reza Sailani M, Baumer A, Schinzel A, Mackay DJ, Robinson DO, Cobellis G, et al. 2010. Methylation profiling in individuals with uniparental disomy identify novel differentially methylated regions on chromosome 15. *Genome Res* **20:** 1271–1278.
Smallwood SA, Tomizawa S, Krueger F, Ruf N, Carli N, Segonds-Pichon A, Sato S, Hata K, Andrews SR, Kelsey G. 2011. Dynamic CpG island methylation landscape in oocytes and pre-implantation embryos. *Nat Genet* **43:** 811–814.
Smith ZD, Chan MM, Mikkelsen TS, Gu H, Gnirke A, Regev A, Meissner A. 2012. A unique regulatory phase of DNA methylation in the early mammalian embryo. *Nature* **484:** 339–344.
Thomson JP, Skene PJ, Selfridge J, Clouaire T, Guy J, Webb S, Kerr AR, Deaton A, Andrews R, James KD, et al. 2010. CpG islands influence chromatin structure via the CpG-binding protein Cfp1. *Nature* **464:** 1082–1086.
Tomizawa S, Kobayashi H, Watanabe T, Andrews S, Hata K, Kelsey G, Sasaki H. 2011. Dynamic stage-specific changes in imprinted differentially methylated regions during early mammalian development and prevalence of non-CpG methylation in oocytes. *Development* **138:** 811–820.
Umlauf D, Goto Y, Cao R, Cerqueira F, Wagschal A, Zhang Y, Feil R. 2004. Imprinting along the *Kcnq1* domain on mouse chromosome 7 involves repressive histone methylation and recruitment of Polycomb group complexes. *Nat Genet* **36:** 1296–1300.
Wood AJ, Schulz R, Woodfine K, Koltowska K, Beechey CV, Peters J, Bourc'his D, Oakey RJ. 2008. Regulation of alternative polyadenylation by genomic imprinting. *Genes Dev* **22:** 1141–1146.
Xie W, Barr CL, Kim A, Yue F, Lee AY, Eubanks J, Dempster EL, Ren B. 2012. Base-resolution analyses of sequence and parent-of-origin dependent DNA methylation in the mouse genome. *Cell* **148:** 816–831.
Yamazawa K, Nakabayashi K, Kagami M, Sato T, Saitoh S, Horikawa R, Hizuka N, Ogata T. 2010. Parthenogenetic chimaerism/mosaicism with a Silver-Russell syndrome-like phenotype. *J Med Genet* **47:** 782–785.
Yuen RKC, Jiang R, Penaherrera M, McFadeen DE, Robinson WP. 2011. Genome-wide mapping of imprinted differentially methylated regions by DNA methylation profiling of human placentas from triploidies. *Epigenetics & Chromatin* **4:** 10.
Zeng J, Konopka G, Hunt BG, Preuss TM, Geschwind D, Yi SV. 2012. Divergent whole-genome methylation maps of human and chimpanzee brains reveal epigenetic basis of human regulatory evolution. *Am J Hum Genet* **91:** 455–465.
Zhang Y, Jurkowska R, Soeroes S, Rajavelu A, Dhayalan A, Bock I, Rathert P, Brandt O, Reinhardt R, Fischle W, et al. 2010. Chromatin methylation activity of Dnmt3a and Dnmt3a/3L is guided by interaction of the ADD domain with the histone H3 tail. *Nucleic Acids Res* **38:** 4246–4253.

Received August 9, 2013; accepted in revised form December 26, 2013.

CLINICAL GENETICS An International Journal of Genetics, Molecular and Personalized Medicine

Clin Genet 2013
Printed in Singapore. All rights reserved

Published by John Wiley & Sons Ltd
CLINICAL GENETICS
doi: 10.1111/cge.12318

Short Report

A novel *de novo* point mutation of the OCT-binding site in the *IGF2/H19*-imprinting control region in a Beckwith–Wiedemann syndrome patient

Higashimoto K, Jozaki K, Kosho T, Matsubara K, Fuke T, Yamada D, Yatsuki H, Maeda T, Ohtsuka Y, Nishioka K, Joh K, Koseki H, Ogata T, Soejima H. A novel *de novo* point mutation of the OCT-binding site in the *IGF2/H19*-imprinting control region in a Beckwith–Wiedemann syndrome patient.
Clin Genet 2013. © John Wiley & Sons A/S. Published by John Wiley & Sons Ltd, 2013

The *IGF2/H19*-imprinting control region (ICR1) functions as an insulator to methylation-sensitive binding of CTCF protein, and regulates imprinted expression of *IGF2* and *H19* in a parental origin-specific manner. ICR1 methylation defects cause abnormal expression of imprinted genes, leading to Beckwith–Wiedemann syndrome (BWS) or Silver–Russell syndrome (SRS). Not only ICR1 microdeletions involving the CTCF-binding site, but also point mutations and a small deletion of the OCT-binding site have been shown to trigger methylation defects in BWS. Here, mutational analysis of ICR1 in 11 BWS and 12 SRS patients with ICR1 methylation defects revealed a novel *de novo* point mutation of the OCT-binding site on the maternal allele in one BWS patient. In BWS, all reported mutations and the small deletion of the OCT-binding site, including our case, have occurred within repeat A2. These findings indicate that the OCT-binding site is important for maintaining an unmethylated status of maternal ICR1 in early embryogenesis.

Conflict of interest

The authors have no competing financial interests to declare.

K Higashimoto[a], K Jozaki[a], T Kosho[b], K Matsubara[c], T Fuke[c], D Yamada[d], H Yatsuki[a], T Maeda[a], Y Ohtsuka[a], K Nishioka[a], K Joh[a], H Koseki[d], T Ogata[e] and H Soejima[a]

[a]Division of Molecular Genetics & Epigenetics, Department of Biomolecular Sciences, Faculty of Medicine, Saga University, Saga, Japan, [b]Department of Medical Genetics, Shinshu University School of Medicine, Matsumoto, Nagano, Japan, [c]Department of Molecular Endocrinology, National Research Institute for Child Health and Development, Tokyo, Japan, [d]Laboratory for Developmental Genetics, RIKEN Center for Integrative Medical Sciences (IMS), Yokohama, Kanagawa, Japan, and [e]Department of Pediatrics, Hamamatsu University School of Medicine, Hamamatsu, Japan

Key words: Beckwith–Wiedemann syndrome – ICR1 methylation defect – *IGF2/H19* – OCT-binding site – Silver–Russell syndrome

Corresponding author: Hidenobu Soejima, Division of Molecular Genetics & Epigenetics, Department of Biomolecular Sciences, Faculty of Medicine, Saga University, 5-1-1 Nabeshima, Saga 849–8501, Japan.
Tel.: +81 952 34 2260;
fax: +81 952 34 2067;
e-mail: soejimah@cc.saga-u.ac.jp

Received 5 August 2013, revised and accepted for publication 6 November 2013

Human 11p15 contains two neighboring imprinted domains, *IGF2/H19* and *KCNQ1*. Each domain is controlled by its own imprinting control region: ICR1 or ICR2, respectively (1). ICR1 methylation defects cause abnormal imprinted expression of insulin-like growth factor 2 (*IGF2*), which encodes a growth factor, and non-coding RNA *H19*, which possesses possible tumor-suppressor functions, leading to Beckwith–Wiedemann syndrome (BWS: OMIM 130650) and Silver–Russell syndrome (SRS: OMIM 180860), respectively (1, 2).

BWS is a congenital overgrowth disorder characterized by macroglossia, macrosomia, and abdominal wall defects, whereas SRS is a congenital growth retardation disorder characterized by a typical facial gestalt, clinodactyly V, and body asymmetry (1, 2). Among varied causative genetic and epigenetic abnormalities, ICR1 methylation defects are etiologies common to both diseases. Gain of methylation (GOM) and loss of methylation (LOM) at ICR1 account for ~5% of BWS and ~44% of SRS cases, respectively (1, 2).

ICR1 upstream of *H19* is a differentially methylated region (DMR) that is methylated exclusively on the paternal allele, and it regulates the imprinted expression of paternally expressed *IGF2* and maternally expressed *H19*. On the maternal allele, unmethylated ICR1 bound by CTCF forms a chromatin insulator that prevents *IGF2* promoter activation by the enhancer downstream of *H19*, resulting in silencing of *IGF2* and activation of *H19*. On the paternal allele, methylation-sensitive CTCF cannot bind to methylated ICR1, resulting in activation of *IGF2* and silencing of *H19* (3, 4). CTCF also maintains the unmethylated status of ICR1 on the maternal allele (5, 6).

Human ICR1 contains two different repetitive sequences (A and B) and seven CTCF-binding sites (CTSs) (Fig. 1a). A maternally inherited ICR1 microdeletion (1.4–2.2 kb), which affects ICR1 function and CTCF binding by changing CTS spacing, has been reported to result in ICR1-GOM in a few familial BWS cases (7–9). ICR1 also contains other protein-binding motifs, such as OCT, SOX, and ZFP57 (10, 11). Recently, point mutations and a small deletion of the OCT or SOX motif have been reported in a few BWS patients with ICR1-GOM (10, 12, 13).

Here, mutational analysis in 11 BWS and 12 SRS patients with ICR1 methylation defects revealed a novel *de novo* point mutation in the OCT-binding site on the maternal allele of one BWS patient.

Materials and methods

Patients

Eleven BWS and twelve SRS patients, who were clinically diagnosed, were enrolled in this study. All BWS and SRS patients displayed isolated GOM and LOM of ICR1, respectively. This study was approved by the Ethics Committee for Human Genome and Gene Analyses of the Faculty of Medicine, Saga University. Written informed consents were obtained from the parents or guardians of the patients.

Sequencing analysis of ICR1

A genomic region in and around ICR1, which included seven CTSs and three OCT-binding sites, was directly sequenced in all patients as previously described (14). All polymerase chain reaction (PCR) primer pairs used are listed in Table S1, Supporting Information.

Microsatellite analysis

For quantitative polymorphism analysis, tetranucleotide repeat markers, *D11S1984* at 11p15.5 and *D11S1997* at 11p15.4, were amplified and analyzed with GeneMapper software. The peak height ratios of the paternal allele to the maternal allele were calculated.

Southern blot analysis

Methylation-sensitive Southern blots with *Pst*I/*Mlu*I and *Bam*HI/*Not*I were employed for ICR1 and ICR2, respectively, as described previously (15). Band intensity was measured using a FLA-7000 fluoro-image analyzer (Fujifilm, Tokyo, Japan). The methylation index (MI, %) was then calculated.

Bisulfite sequencing

Bisulfite sequencing was performed covering the three variants within ICR1 that were found in BWS-s043. Genomic DNA was bisulfite-converted using an EpiTect Bisulfite Kit (Qiagen, Hilden, Germany). After PCR amplification, the products were cloned and sequenced.

Electrophoretic mobility shift assay

The pCMX-Flag-human OCT4 and pCMX-Flag-human SOX2 were simultaneously transfected into HEK293 cells. The nuclear extracts from HEK293 cells expressing human OCT4/SOX2 and mouse ES cells were used. Electrophoretic mobility shift assay (EMSA) was performed as described previously (10). For supershift analysis, 1.5 µg of anti-OCT4 antibody (Abcam, ab19857, Cambridge, UK) or 1.5 µg of anti-SOX2 antibody (R&D systems, AF2018, Minneapolis, MN) was used. The unlabeled probes were also used as competitors. The reaction mixtures were separated on a 4% polyacrylamide gel and exposed to a film. Oligonucleotide sequences are presented in Table S1.

Results

Among 11 BWS and 12 SRS patients with ICR1 methylation defects, 7 and 2 variants from 5 BWS and 2 SRS patients were found, respectively (Table 1). The variants in BWS-047 and BWS-s061 were polymorphisms. The remaining variants were not found in the normal population, the UCSC Genome Browser database, or the 1000 Genomes database, suggesting them to be candidates for causative mutations for ICR1 methylation defects. However, the positions of the variants, except

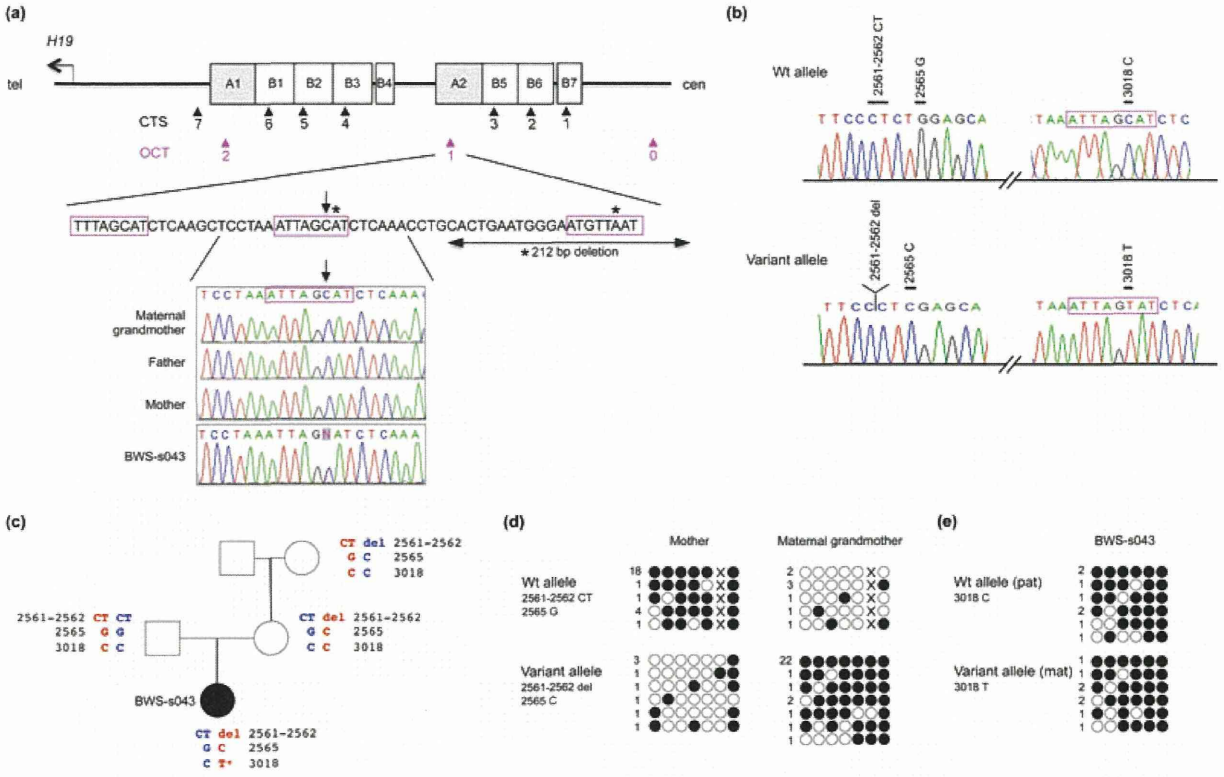

Fig. 1. The three variants in BWS-s043 and their effects on ICR1 methylation. (**a**) Map of ICR1 and the position of 2,023,018C>T. Upper panel: structure of ICR1. ICR1 consists of two repeat blocks. Each block consists of one repeat A and three or four repeat Bs. The black and red arrowheads indicate CTCF-binding sites (CTS) and OCT-binding sites (OCT), respectively. Middle panel: the position of 2,023,018C>T (arrow) and previously reported mutations and deletions (asterisks). Three octamer motifs are enclosed by a red line. Lower panel: electrophoretograms around 2,023,018C>T. BWS-s043 were heterozygous for the variant, whereas the maternal grandmother and both parents did not harbor it. (**b**) Haplotype encompassing the three variants in BWS-s043. Polymerase chain reaction (PCR) products encompassing the three variants were cloned and sequenced. All three variants were revealed to be on the same allele in BWS-s043. (**c**) Pedigree and haplotype of the family. Haplotype analysis showed that 2,023,018C>T (asterisk) occurred on the maternal allele in BWS-s043. (**d**) Bisulfite sequencing analysis encompassing the 2,022,561-562CT>delCT and the 2,022,565G>C variants in the mother and the maternal grandmother. Open and filled circles indicate unmethylated and methylated CpG sites, respectively. X indicates G at chr11: 2,022,565. Numerals on the left reflect the number of clones with the same methylation pattern. The variant allele was unmethylated in the mother and methylated in the maternal grandmother, respectively. (**e**) Bisulfite sequencing analysis encompassing 2,023,018C>T in BWS-s043. The maternal allele contained a *de novo* variant that was heavily methylated in BWS-s043, while differential methylation was maintained in other family members and normal controls without the variant (Fig. S2a).

Table 1. Variants found in this study[a]

Patient ID	MI of ICR1 (%)	Variant	Position (GRCh37/hg19 chr11)	Location	Transmission	Heterozygosity in normal population
BWS-047	100	G>Gdel	2,024,428	Centromeric outside of ICR1 (5′ of CTS1)	Maternal	2/116 (rs200288360)
		CT>CT del	2,022,561–2,022,562	Between A2 and B4	Maternal	na
BWS-s043	86	G>C	2,022,565	Between A2 and B4	Maternal	0/115
		C>T	2,023,018	A2 (OCT-binding site 1)	*De novo*	0/107
BWS-s061	76	C>T	2,023,497	B5 (5′ of CTS3)	Paternal	2/105
BWS-s081	67	C>T	2,025,777	Centromeric outside of ICR1 (3′ of OCT-binding site 0)	Paternal	0/106
BWS-s100	67	C>A	2,021,145	B1 (3′ of CTS6)	Maternal	0/105
SRS-002	4	G>Gdel	2,024,364	B7 (5′ of CTS1)	Unknown	0/106
SRS-s03	24	C>T	2,021,103	B1 (3′ of CTS6)	Maternal	0/106

ICR, imprinting control region; MI, methylation index; na, not analyzed.
[a]Parents' DNA were not available for SRS-002.

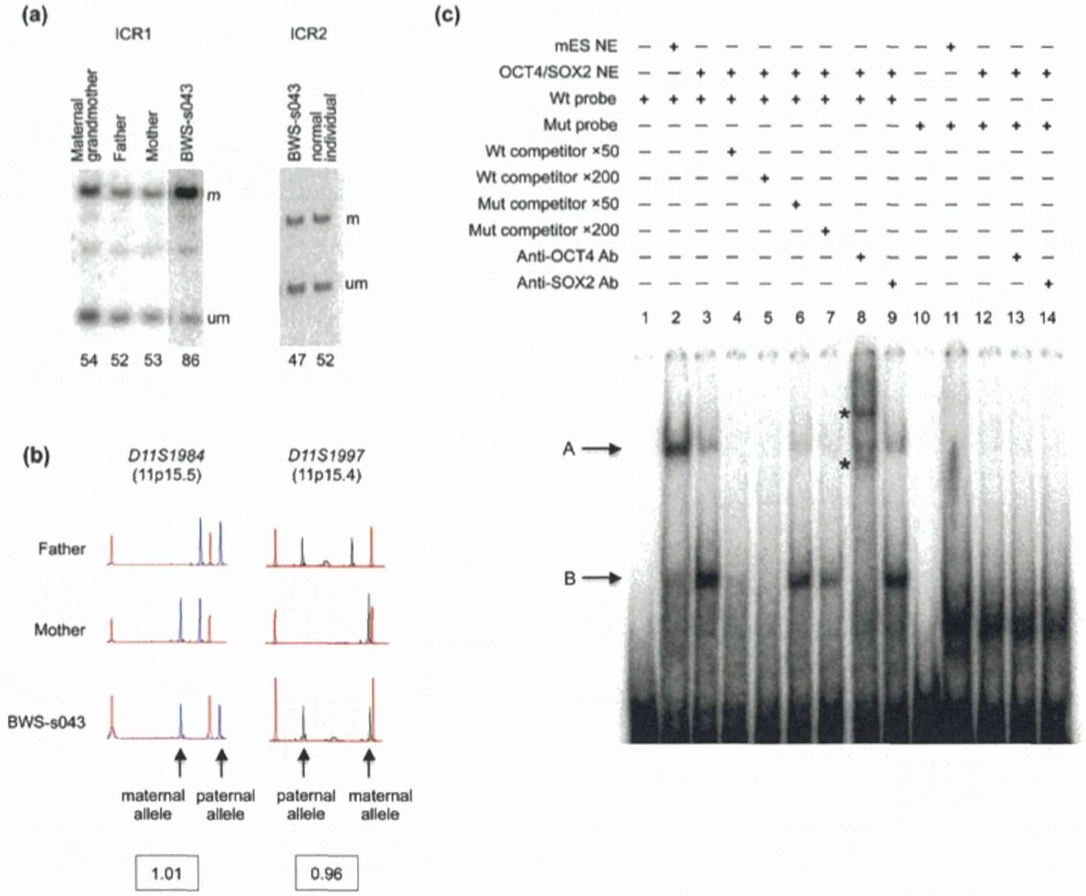

Fig. 2. Methylation-sensitive Southern blots and microsatellite analysis of BWS-s043, and electrophoretic mobility shift assay (EMSA) for 2,023,018C>T. (**a**) Methylation-sensitive Sothern blots of ICR1 and ICR2. Methylation indices [MI, %] are shown below each lane. MI was calculated using the equation $M/(M+U) \times 100$, where M is the intensity of the methylated band and U is the intensity of the unmethylated band. m, methylated band; um, unmethylated band. BWS-s043 showed ICR1-GOM, whereas the relatives did not. Methylation statuses of CTS1 and CTS4 are shown in Fig. S2b,c. Methylation of ICR2 in BWS-s043 was normal. (**b**) Microsatellite analysis at 11p15.4-p15.5. Ratios of the paternal allele to the maternal allele in BWS-s043 were approximately 1, indicating no uniparental disomy. Red peaks are molecular markers. (**c**) EMSA using the wild-type (Wt) probe and the mutant (Mut) probe encompassing 2,023,018C>T. The unlabeled Wt probe or Mut probe (×50 or ×200 molar excess) was used as a competitor. The arrows and asterisks indicate the protein-DNA complexes (A and B) and supershifted complexes, respectively. mES NE, nuclear extract from mouse ES cells; OCT4/SOX2 NE, nuclear extract from human HEK293 cells expressing OCT4/SOX2; Ab, antibody.

for BWS-s043, were not located at any protein-binding sites that have been reported as involved in methylation imprinting (CTCF, OCT, and ZFP57) (3, 4, 10, 12, 16). Furthermore, we did not find any protein-oligonucleotide complexes in EMSA using mouse ES nuclear extracts and oligonucleotide probes encompassing all variants, except for BWS-s043 (Fig. S1). Therefore, we analyzed further three variants in BWS-s043, which were in and around the OCT-binding site 1.

First, we re-confirmed that BWS-s043 showed GOM near CTS6 within ICR1, but it did not demonstrate LOM at ICR2, paternal uniparental disomy of chromosome 11, or a *CDKN1C* mutation (Fig. 2a,b, and data not shown). The 2,023,018C>T variant was located in the second octamer motif of OCT-binding site 1 within repeat A2 (Fig. 1a). The other two variants were located approximately 450 bp on the telomeric side of the 2,023,018C>T variant, between repeats A2 and B4 (Fig. 1a, Table 1). The 2,023,018C>T variant was absent in other family members, indicating a *de novo* variant (Fig. 1a). To clarify if the *de novo* variant in the patient occurred on the maternal or paternal allele, we performed haplotype analysis with PCR covering all three variants. We found all three variants were located on the same allele and the 2,023,018C>T variant occurred *de novo* on the maternal allele because the 2,022,561–562CT>delCT and 2,022,565G>C variants were on the maternal allele in the patient (Fig. 1b,c).

Next, we investigated the methylation status of ICR1. Methylation-sensitive Southern blots and bisulfite sequencing showed normal methylation of ICR1 in the parents and the maternal grandmother (Figs 2a and S2). As for the 2,022,561-562CT>delCT and the 2,022,565G>C variants, the variant allele was unmethylated in the mother, but methylated in the grandmother (Fig. 1d). On the basis of methylation

analysis, the variant allele in the grandmother must have been transmitted by her father, and that in the mother must have been transmitted by her mother. The results indicated that the variant allele could be either methylated or unmethylated during gametogenesis, strongly suggesting no relation between the variants and ICR1-GOM. On the other hand, bisulfite sequencing including the 2,023,018C>T variant revealed that both the variant and wild-type alleles were heavily methylated in the patient (Fig. 1e), while differential methylation was maintained in other family members and normal controls without the variant (Fig. S2a). As the *de novo* variant on the maternal allele was located within the OCT-binding site, which is required for the maintenance of the unmethylated status in a mouse model, the variant was likely involved in ICR1-GOM (17, 18).

Finally, we performed EMSA to determine if 2,023,018C>T influenced the binding ability of nuclear protein factors, such as OCT4 and SOX2 (Fig. 2c). The wild-type probe formed two complexes (A and B) with the nuclear extracts of mouse ES cells and HEK293 cells expressing OCT4/SOX2 (lanes 2 and 3), whereas such complexes were not observed in the mutant probe (lanes 11 and 12). Complexes A and B competed more efficiently with wild-type than with the mutant competitor (lanes 4 to 7). Furthermore, complex B, but not A, was supershifted with the antibody against OCT4 (lane 8). The supershift did not occur with the antibody against SOX2 and with both antibodies using the mutant probe (lanes 9, 13, and 14). These data demonstrated that 2,023,018C>T abrogated binding ability of a nuclear factor, most likely OCT4. Taken together, our data strongly suggest that 2,023,018C>T is a mutation that could prevent OCT4 binding to the OCT-binding site and induce ICR1-GOM, leading to BWS.

Discussion

We identified a novel *de novo* point mutation, chr11: 2,023,018C>T, in OCT-binding site 1 within repeat A2 in a BWS patient with ICR1-GOM. Our data strongly suggest the involvement of the mutation in GOM at ICR1. In a mouse cell model, the evolutionarily well-conserved dyad octamer motif within ICR1, which is bound by OCT protein, has been shown to be required for the maintenance of unmethylated status competing against *de novo* methylation (17). In addition, the importance of a SOX motif flanked by an OCT motif has also been reported (19). Recent studies have shown that the SOX–OCT motif functions to maintain unmethylated status *in vitro* and *in vivo*; a cooperative function of CTCF and OCT/SOX for maintenance of differential methylation has been suggested as responsible (18, 19). Although there is one OCT-binding site in mice, three evolutionarily conserved OCT-binding sites (0, 1, 2) are located in and around ICR1 in humans. As all mutations and the small deletion previously reported in addition to our case occurred in site 1 within repeat A2 (Fig. 1a), site 1 within repeat A2 likely plays a more important role for maintaining unmethylated status of maternal ICR1 in humans than the other OCT-binding sites (10, 12, 13).

ICR1-GOM cases, including ours, with mutations/deletions also show partial hypermethylation in spite of pre-existent genetic aberrations in the oocyte (9, 12, 13, 20), suggesting aberrant hypermethylation at ICR1 would also be stochastically acquired at a cellular level even in the existence of such aberrations.

As for SRS, including familial cases, the ICR1 mutation has not been found except in one sporadic case to date (10). We did not find any promising mutations in this study, suggesting the cause of ICR1 methylation defects to differ between SRS and BWS.

In conclusion, we identified a novel *de novo* point mutation of OCT-binding site 1 within repeat A2, a location suggested to play an important role for maintaining the unmethylated status of maternal ICR1 in humans, on the maternal allele in a BWS patient with ICR1-GOM. However, genetic aberrations of ICR1 explain only 20% of BWS cases with ICR1-GOM (10). As aberrant methylation may occur as a consequence of stochastic events or environmental influences irrespective of ICR1 mutations, unknown causes for ICR1 methylation defects should be clarified.

Supporting Information

The following Supporting information is available for this article:

Fig. S1. EMSA for all variants found in this study, except for those in BWS-047 and BWS-s061, using the nuclear extract from mouse ES cells. The variant in BWS-s081 was located outside of ICR1, and a CpG site within the probe sequence was mostly unmethylated in three normal controls (data not shown). Thus, an unmethylated probe was used for it. Since the variants in BWS-s100 and SRS-s03 were located 3′ of CTS6 and found on the maternal allele, unmethylated probes were used for them. As for the variant in SRS-002, it was located 5′ of CTS1 but its parental origin was unknown. Thus, both unmethylated and methylated probes were used for it. There was no difference between a wt-probe and a variant-probe in each variant except for the BWS-s043 mutation. A wt-probe for the BWS-s043 mutation formed two complexes, whereas such complexes were not observed with a probe for the mutation. These results suggested that only the BWS-s043 mutation affected the protein–DNA interaction (see text and Fig. 2c for details). WT, probe for the wild-type sequence; MUT, probe for the BWS-s043 mutation; VAR, probe for the variant sequence; um, unmethylated probe; me, methylated probe; mES NE, nuclear extract from mouse ES cells. *Fig. S2*. Bisulfite sequencing of the region encompassing the 2,023,018 variant, CTS1, and CTS4. (**a**) Results for the 2,023,018 variant. In the healthy members of the BWS-s043 family, comprised of the maternal grandmother, mother, and father, showed differential methylation. Three normal controls also showed differential methylation. In particular, normal control 3 was heterozygous for a SNP (rs61520309) and showed differential methylation in an allele-dependent manner. Open and filled circles indicate unmethylated and methylated CpG sites, respectively. (**b**) Results for CTS1. Two normal controls that were heterozygous for a SNP (rs2525885) showed differential methylation. The healthy family members also showed differential methylation, whereas the patient, BWS-s043, showed aberrant hypermethylation. CpG sites within CTS1 are indicated by a short horizontal line. X indicates T of the SNP (rs2525885). (**c**) Results for CTS4. The healthy family members and two normal controls showed differential

methylation. Among them, the parents and two normal controls were heterozygous for a SNP (rs2525883). The patient, BWS-s043, showed aberrant hypermethylation. CpG sites within CTS4 were indicated by a short horizontal line. X indicates T of the SNP (rs2525883).
Table S1. PCR primers and oligonucleotide probes used in this study.

Additional Supporting information may be found in the online version of this article.

Acknowledgements

This study was supported, in part, by a Grant for Research on Intractable Diseases from the Ministry of Health, Labor, and Welfare; a Grant for Child Health and Development from the National Center for Child Health and Development; a Grant-in-Aid for Challenging Exploratory Research; and, a Grant-in-Aid for Scientific Research (C) from the Japan Society for the Promotion of Science.

References

1. Weksberg R, Shuman C, Beckwith JB. Beckwith–Wiedemann syndrome. Eur J Hum Genet 2010: 18: 8–14.
2. Gicquel C, Rossignol S, Cabrol S et al. Epimutation of the telomeric imprinting center region on chromosome 11p15 in Silver–Russell syndrome. Nat Genet 2005: 37: 1003–1007.
3. Bell AC, Felsenfeld G. Methylation of a CTCF-dependent boundary controls imprinted expression of the Igf2 gene. Nature 2000: 405: 482–485.
4. Hark AT, Schoenherr CJ, Katz DJ, Ingram RS, Levorse JM, Tilghman SM. CTCF mediates methylation-sensitive enhancer-blocking activity at the H19/Igf2 locus. Nature 2000: 405: 486–489.
5. Schoenherr CJ, Levorse JM, Tilghman SM. CTCF maintains differential methylation at the Igf2/H19 locus. Nat Genet 2003: 33: 66–69.
6. Pant V, Mariano P, Kanduri C et al. The nucleotides responsible for the direct physical contact between the chromatin insulator protein CTCF and the H19 imprinting control region manifest parent of origin-specific long-distance insulation and methylation-free domains. Genes Dev 2003: 17: 586–590.
7. Sparago A, Cerrato F, Vernucci M, Ferrero GB, Silengo MC, Riccio A. Microdeletions in the human H19 DMR result in loss of IGF2 imprinting and Beckwith–Wiedemann syndrome. Nat Genet 2004: 36: 958–960.
8. Prawitt D, Enklaar T, Gärtner-Rupprecht B et al. Microdeletion of target sites for insulator protein CTCF in a chromosome 11p15 imprinting center in Beckwith–Wiedemann syndrome and Wilms' tumor. Proc Natl Acad Sci U S A 2005: 102: 4085–4090.
9. Beygo J, Citro V, Sparago A et al. The molecular function and clinical phenotype of partial deletions of the IGF2/H19 imprinting control region depends on the spatial arrangement of the remaining CTCF-binding sites. Hum Mol Genet 2013: 22: 544–557.
10. Demars J, Shmela ME, Rossignol S et al. Analysis of the IGF2/H19 imprinting control region uncovers new genetic defects, including mutations of OCT-binding sequences, in patients with 11p15 fetal growth disorders. Hum Mol Genet 2010: 19: 803–814.
11. Quenneville S, Verde G, Corsinotti A et al. In embryonic stem cells, ZFP57/KAP1 recognize a methylated hexanucleotide to affect chromatin and DNA methylation of imprinting control regions. Mol Cell 2011: 44: 361–372.
12. Poole RL, Docherty LE, Al Sayegh A et al. Targeted methylation testing of a patient cohort broadens the epigenetic and clinical description of imprinting disorders. Am J Med Genet A 2013: 161: 2174–2182.
13. Berland S, Appelbäck M, Bruland O et al. Evidence for anticipation in Beckwith–Wiedemann syndrome. Eur J Hum Genet 2013: 21: 1344–1348.
14. Higashimoto K, Nakabayashi K, Yatsuki H et al. Aberrant methylation of H19-DMR acquired after implantation was dissimilar in soma versus placenta of patients with Beckwith–Wiedemann syndrome. Am J Med Genet A 2012: 158A: 1670–1675.
15. Soejima H, Nakagawachi T, Zhao W et al. Silencing of imprinted CDKN1C gene expression is associated with loss of CpG and histone H3 lysine 9 methylation at DMR-LIT1 in esophageal cancer. Oncogene 2004: 23: 4380–4388.
16. Mackay DJ, Callaway JL, Marks SM et al. Hypomethylation of multiple imprinted loci in individuals with transient neonatal diabetes is associated with mutations in ZFP57. Nat Genet 2008: 40: 949–951.
17. Hori N, Nakano H, Takeuchi T et al. A dyad Oct-binding sequence functions as a maintenance sequence for the unmethylated state within the H19/Igf2-imprinted control region. J Biol Chem 2002: 277: 27960–27967.
18. Sakaguchi R, Okamura E, Matsuzaki H, Fukamizu A, Tanimoto K. Sox-Oct motifs contribute to maintenance of the unmethylated H19 ICR in YAC transgenic mice. Hum Mol Genet 2013: 22: 4627–4637.
19. Hori N, Yamane M, Kouno K, Sato K. Induction of DNA demethylation depending on two sets of Sox2 and adjacent Oct3/4 binding sites (Sox-Oct motifs) within the mouse H19/insulin-like growth factor 2 (Igf2) imprinted control region. J Biol Chem 2012: 287: 44006–44016.
20. Sparago A, Russo S, Cerrato F et al. Mechanisms causing imprinting defects in familial Beckwith–Wiedemann syndrome with Wilms' tumour. Hum Mol Genet 2007: 16: 254–264.

Clinical Endocrinology (2013) doi: 10.1111/cen.12379

ORIGINAL ARTICLE

IMAGe syndrome: clinical and genetic implications based on investigations in three Japanese patients

Fumiko Kato*, Takashi Hamajima†, Tomonobu Hasegawa‡, Naoko Amano‡, Reiko Horikawa§, Gen Nishimura¶, Shinichi Nakashima*, Tomoko Fuke**, Shinichirou Sano**, Maki Fukami** and Tsutomu Ogata*

*Department of Pediatrics, Hamamatsu University School of Medicine, Hamamatsu, †Division of Endocrinology and Metabolism, Aichi Children's Health and Medical Center, Obu, ‡Department of Pediatrics, Keio University School of Medicine, §Division of Endocrinology and Metabolism, National Center for Child Health and Development, Tokyo, ¶Department of Radiology, Tokyo Metropolitan Children's Medical Center, Fuchu, and **Department of Molecular Endocrinology, National Research Institute for Child Health and Development, Tokyo, Japan

Summary

Objective Arboleda *et al.* have recently shown that IMAGe (intra-uterine growth restriction, metaphyseal dysplasia, adrenal hypoplasia congenita and genital abnormalities) syndrome is caused by gain-of-function mutations of maternally expressed gene *CDKN1C* on chromosome 11p15.5. However, there is no other report describing clinical findings in patients with molecularly studied IMAGe syndrome. Here, we report clinical and molecular findings in Japanese patients.

Patients We studied a 46,XX patient aged 8·5 years (case 1) and two 46,XY patients aged 16·5 and 15·0 years (cases 2 and 3).

Results Clinical studies revealed not only IMAGe syndrome-compatible phenotypes in cases 1–3, but also hitherto undescribed findings including relative macrocephaly and apparently normal pituitary-gonadal endocrine function in cases 1–3, familial glucocorticoid deficiency (FGD)-like adrenal phenotype and the history of oligohydramnios in case 2, and arachnodactyly in case 3. Sequence analysis of *CDKN1C*, pyrosequencing-based methylation analysis of KvDMR1 and high-density oligonucleotide array comparative genome hybridization analysis for chromosome 11p15.5 were performed, showing an identical *de novo* and maternally inherited *CDKN1C* gain-of-function mutation (p.Asp274Asn) in cases 1 and 2, respectively, and no demonstrable abnormality in case 3.

Conclusions The results of cases 1 and 2 with *CDKN1C* mutation would argue the following: [1] relative macrocephaly is consistent with maternal expression of *CDKN1C* in most tissues and biparental expression of *CDKN1C* in the foetal brain; [2] FGD-like phenotype can result from *CDKN1C* mutation; and [3] genital abnormalities may primarily be ascribed to placental dysfunction. Furthermore, lack of *CDKN1C* mutation in case 3 implies genetic heterogeneity in IMAGe syndrome.

(Received 1 October 2013; returned for revision 24 November 2013; finally revised 26 November 2013; accepted 29 November 2013)

Introduction

IMAGe syndrome is a multisystem developmental disorder named by the acronym of intra-uterine growth restriction (IUGR), metaphyseal dysplasia and adrenal hypoplasia congenita common to both 46,XY and 46,XX patients, and genital abnormalities specific to 46,XY patients.[1] In addition to these salient clinical features, hypercalciuria has been reported frequently in IMAGe syndrome.[1,2] This condition occurs not only as a sporadic form but also as a familial form.[1–3] Furthermore, transmission analysis in a large pedigree has revealed an absolute maternal inheritance of this condition, indicating the relevance of a maternally expressed gene to the development of IMAGe syndrome.[3]

Subsequently, Arboleda *et al.*[4] have mapped the causative gene to a ~17·2-Mb region on chromosome 11 by an identity-by-descent analysis in this large pedigree and performed targeted exon array capture and high-throughput genomic sequencing for this region in the affected family members and in other sporadic patients. Consequently, they have identified five different missense mutations in the maternally expressed gene *CDKN1C* (cyclin-dependent kinase inhibitor 1C) that resides on the imprinting control region 2 (ICR2) domain at chromosome 11p15.5 and encodes a negative regulator for cell proliferation.[4–6] Notably, all the missense mutations are clustered within a specific segment of PCNA-binding domain, and functional studies have implicated that these mutations have gain-of-function effects.[4] Thus, IMAGe syndrome appears to constitute a mirror image of Beckwith–Wiedemann syndrome (BWS) in terms of the

Correspondence: Dr. Tsutomu Ogata, Department of Pediatrics, Hamamatsu University School of Medicine, 1-20-1 Handayama, Higashi-ku, Hamamatsu 431-3192, Japan. Tel./Fax: +81 53 435 2310; E-mail: tomogata@hama-med.ac.jp

CDKN1C function, because multiple *CDKN1C* loss-of-function mutations have been identified in BWS with no mutation shared in common by IMAGe syndrome and BWS.[4,5]

However, several matters remain to be clarified in IMAGe syndrome, including phenotypic spectrum and underlying mechanism(s) for the development of each phenotype in *CDKN1C*-mutation-positive patients, and the presence or absence of genetic heterogeneity. Here, we report clinical and molecular findings in three patients with IMAGe syndrome and discuss these unresolved matters.

Patients and methods

Patients

We studied one previously described 46,XX patient (case 1)[7] and two hitherto unreported 46,XY patients (cases 2 and 3). In cases 1–3, no pathologic mutations were identified in the coding exons and their splice cites of *NR5A1* (*SF1*) and *NR0B1* (*DAX1*) relevant to adrenal hypoplasia,[8] and *MC2R*, *MRAP*, *STAR* and *NNT* involved in familial glucocorticoid deficiency (FGD).[9]

Ethical approval and samples

This study was approved by the Institutional Review Board Committee at Hamamatsu University School of Medicine. Molecular studies were performed using leucocyte genomic DNA samples of cases 1–3 and the parents of cases 1 and 2, after obtaining written informed consent.

Sequence analysis of CDKN1C

The coding exons 1 and 2 and their flanking splice sites were amplified by polymerase chain reaction (PCR) (Fig. 1a), using primers shown in Table S1. Subsequently, the PCR products were subjected to direct sequencing from both directions on ABI 3130 autosequencer (Life Technologies, Carlsbad, CA, USA). In this regard, if a nucleotide variation were present within the primer-binding site(s), this may cause a false-negative finding because of amplification failure of a mutation-positive allele. Thus, PNCA-binding domain was examined with different primer sets. To confirm a heterozygous mutation, the corresponding PCR products were subcloned with TOPO TA Cloning Kit (Life Technologies), and normal and mutant alleles were sequenced separately.

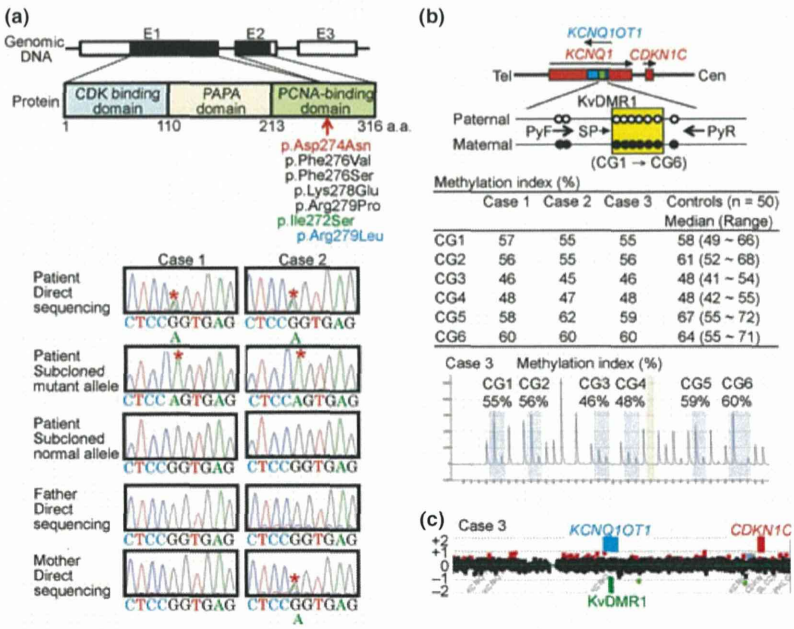

Fig. 1 Summary of molecular studies. (a) Sequence analysis of *CDKN1C*. *CDKN1C* consists of three exons (E1–E3), and the black and white boxes denote the coding regions and the untranslated regions, respectively. CDKN1C protein is composed of 316 amino acids and contains CDK binding domain, PAPA domain and PCNA-binding domain. The p.Asp274Asn mutation found in this study and the previous study[4] is shown in red. The four mutations written in black have also been identified in IMAGe syndrome.[4] The pIle272Ser mutation written in green has been detected in atypical IMAGe syndrome lacking skeletal lesion,[22] and the pArg279Leu mutation written in blue has been found in SRS.[24] Electrochromatograms denote a *de novo* p.Asp274Asn mutation in case 1 and a maternally inherited p.Asp274Asn mutation in case 2. (b) Methylation analysis of KvDMR1 at the ICR2 domain. The cytosine residues at the CpG dinucleotides are unmethylated after paternal transmission (open circles) and methylated after maternal transmission (filled circles). *KCNQ1OT1* is a paternally expressed gene, and *KCNQ1* and *CDKN1C* are maternally expressed genes. The six CpG dinucleotides (CG1→CG6) examined by pyrosequencing are highlighted with a yellow rectangle, and the positions of PyF & PyR primers and SP are shown by thick arrows and a thin arrow, respectively. A pyrogram of case 3 is shown. (c) Array CGH analysis for chromosome 11p15.5 encompassing the ICR2 domain in case 3. A region encompassing KvDMR1 and *CDKN1C* is shown. Black, red and green dots denote signals indicative of the normal, the increased (>+0·5) and the decreased (<−1·0) copy numbers, respectively. Although several red and green signals are seen, there is no portion associated with ≥3 consecutive red or green signals.

Methylation analysis of KvDMR1 and array CGH analysis for chromosome 11p15.5

Increased expression of *CDKN1C*, as well as gain-of-function mutations of *CDKN1C*, may lead to IMAGe syndrome. Such increased *CDKN1C* expression would occur in association with hypermethylated KvDMR1 (differentially methylated region 1) at the ICR2 domain, because *CDKN1C* is expressed when the *cis*-situated KvDMR1 is methylated as observed after maternal transmission and is repressed when the *cis*-situated KvDMR1 is unmethylated as observed after paternal transmission.[5] Thus, we performed pyrosequencing analysis for six CpG dinucleotides (CG1–CG6) within KvDMR1, using bisulphite-treated leucocyte genomic DNA samples (Fig. 1b). In brief, a 155-bp region was PCR-amplified with a primer set (PyF and PyR) for both methylated and unmethylated clones, and a sequence primer (SP) was hybridized to single-stranded PCR products (for PyF, PyR and SP sequences, see Table S1). Subsequently, methylation index (MI, the ratio of methylated clones) was obtained for each CpG dinucleotide, using PyroMark Q24 (Qiagen, Hilden, Germany). To define the reference ranges of MIs, 50 control subjects were similarly studied with permission.

Increased *CDKN1C* expression may also result from a copy number gain of the maternally inherited ICR2 domain. Thus, we performed high-density array CGH (comparative genomic hybridization) using a custom-build 33 088 oligonucleotide probes for chromosome 11p15.5 encompassing the ICR2 domain, together with ~10 000 reference probes for other chromosomal regions (Agilent Technologies, Santa Clara, CA, USA). The procedure was carried out as described in the manufacturer's instructions.

Results

Clinical findings

Detailed clinical findings are shown in Table 1. Cases 1–3 exhibited characteristic faces with frontal bossing, flat nasal root, low set ears and mild micrognathia, as well as short limbs. They had IUGR and postnatal growth failure. Notably, while birth and present length/height and weight were severely compromised, birth and present occipitofrontal circumference (OFC) were relatively well preserved. Radiological examinations revealed generalized osteopenia, delayed bone maturation and metaphyseal dysplasia with vertical sclerotic striations of the knee in cases 1–3, slender bones in cases 1 and 2, scoliosis in cases 2 and 3, arachnodactyly in case 3 and broad distal phalanx of the thumbs and great toes in case 2 (Fig. 2). Cases 1 and 3 experienced adrenal crisis in early infancy and received glucocorticoid and mineralocorticoid supplementation therapy since infancy. Case 2 had transient neonatal hyponatremia and several episodes of hypoglycaemia without electrolyte abnormality in childhood and was found to have hypoglycaemia and hyponatremia without hyperkalemia when he had severe viral gastroenteritis at 15·5 years of age. Thus, an adrenocorticotropic hormone stimulation test was performed after recovery from gastroenteritis, revealing poor cortisol response. Thereafter, he was placed on glucocorticoid supplementation therapy. As serum electrolytes were normal, mineralocorticoid supplementation therapy was not initiated. Genital abnormalities included cryptorchidism and small testes in cases 2 and 3, and hypospadias in case 3. However, pituitary-gonadal endocrine function was apparently normal in cases 1–3. Urine calcium secretion was borderline high or increased in cases 1–3, although serum calcium and calcium homeostasis-related factors were normal. In addition, feeding difficulties during infancy were observed in cases 1 and 2, but not in case 3, and oligohydramnios was noticed during the pregnancy of case 2. There was no body asymmetry in cases 1–3. Thus, clinical studies in cases 1–3 revealed not only IMAGe syndrome-compatible phenotypes, but also hitherto undescribed clinical finding (Table 2).

Sequence analysis of CDKN1C

A heterozygous identical missense mutation (c.820G>A, p.Asp274Asn) was identified in cases 1 and 2 (Fig. 1a). This mutation occurred as a *de novo* event in case 1 and was inherited from the phenotypically normal mother in case 2. No demonstrable mutation was identified in case 3.

Methylation analysis of KvDMR1 and array CGH analysis for chromosome 11p15.5

The MIs for CG1–CG6 were invariably within the normal range in cases 1–3 (Fig. 1b), and no discernible copy number alteration was identified in cases 1–3 (Fig. 1c). The results excluded maternal uniparental disomy involving KvDMR1, hypermethylation (epimutation) of the paternally inherited KvDMR1 and submicroscopic duplication involving the maternally derived ICR2 domain, as well as submicroscopic deletion affecting the paternally derived ICR2 domain.

Discussion

CDKN1C mutations in IMAGe syndrome

We identified a heterozygous *CDKN1C* missense mutation (Asp274Asn) in cases 1 and 2. This mutation has previously been detected in a patient with IMAGe syndrome.[4] Furthermore, *de novo* occurrence of the mutation in case 1 argues for the mutation being pathologic, and maternal transmission of the mutation in case 2 is consistent with *CDKN1C* being a maternally expressed gene. Thus, our results provide further evidence for specific missense mutations of *CDKN1C* being responsible for the development of IMAGe syndrome.

Clinical features in CDKN1C*-mutation-positive cases 1 and 2*

Several matters are noteworthy with regard to clinical findings in *CDKN1C*-mutation-positive cases 1 and 2. First, although

Table 1. Clinical findings of cases 1–3

	Case 1*	Case 2	Case 3
Karyotype	46,XX	46,XY	46,XY
Present age (year)	8·5	16·5	15·0
Characteristic face	Yes	Yes	Yes
Pre- and postnatal growth			
Gestational age (week)	35	37	38
Birth length (cm) (SDS)	37·0 (−3·5)	40·0 (−4·0)	41·0 (−4·3)
Birth weight (kg) (SDS)	1·34 (−2·9)	2·03 (−3·5)	1·71 (−3·4)
Birth OFC (cm) (SDS)	30·7 (−0·3)	32·0 (−0·9)	33·0 (−0·1)
Birth BMI (kg/m^2) (percentile)	9·8 (<3)	12·7 (50)	10·1 (<3)
BMI (kg/m^2) at 2 years of age (SDS)	14·2 (−1·8)	13·0 (−3·4)	Unknown
Present height (cm) (SDS)	92·8 (−6·2)	124·7 (−7·8)	135·2 (−5·1)
Present weight (kg) (SDS)	16·0 (−1·9)	25·4 (−3·5)	30·4 (−2·6)
Present OFC (cm) (SDS)	52·0 (−0·2)	53·0 (−2·5)	Unknown
Present BMI (kg/m^2) (SDS)	18·6 (+1·6)	16·3 (−2·6)	16·6 (−1·7)
Skeletal abnormality			
Examined age (year)	5·5	16·5	15·0
Generalized osteopenia	Yes	Yes	Yes
Delayed maturation	Yes	Yes	Yes
Metaphyseal dysplasia	Yes	Yes	Yes
Slender bones	Yes	Yes	No
Scoliosis	No	Yes	Yes
Arachnodactyly	No	No	Yes
Broad thumbs & big toes	No	Yes	No
Adrenal dysfunction			
Examined age (year) before therapy	0·1 (39 days)	15·5	0·5 (6 months)
MRI/CT	Undetectable	Undetectable	Undetectable
ACTH (pg/ml)	9010 [19·9 ± 8·8]	427 [22·9 ± 6·2]	>1000 [22·9 ± 6·2]
Cortisol (μg/dl)	8·4 [8·3 ± 3·4]	6·9 [9·5 ± 2·9]	<1·0 [9·5 ± 2·9]
After ACTH stimulation†	N.E.	9·4 [> 20]	<1·0 [> 20]
Plasma renin activity (ng/ml/h)	N.E.	6·0 [1·0 ± 0·1]	>25 [1·01 ± 0·14]
Active renin concentration (pg/ml)	21 400 [2·5–21·4]	N.E.	N.E.
Aldosterone (ng/dl)	6·9 [9·7 ± 4·5]	5·2 [8·5 ± 1·4]	4·1 [7·4 ± 2·2]
Na (mEq/l)	122 [135–145]	141 (127‡) [135–145]	126 [135–145]
K (mEq/l)	8·0 [3·7–4·8]	4·2 (4·0‡) [3·7–4·8]	6·5 [3·7–4·8]
Cl (mEq/l)	86 [98–108]	103 (98‡) [98–108]	89 [98–108]
Glucocorticoid therapy	Yes (since 2 months)	Yes (since 15·5 years)	Yes (since 6 months)
Mineralocorticoid therapy	Yes (since 2 months)	No	Yes (since 6 months)
Genital abnormality			
Examined age (year)	8·5	16·5	15·0
Hypospadias	–	No	Yes (operated at 2 years)
Cryptorchidism	–	Yes (B) (operated at 2 years)	Yes (operated at 2 years)
Micropenis	–	No	No
Testis size (R & L) (ml)	–	5 & 8 [13–20]	4 & 10 [11–20]
Pubic hair (Tanner stage)	1 [10·0 ± 1·4 years]§	4 [14·9 ± 0·9 years]¶	4 [14·9 ± 0·9 years]¶
LH (mIU/ml)	<0·1 [<0·1–1·3]	3·9 [0·2–7·8]	4·8 [0·2–7·8]
After GnRH-stimulation**	3·5 [1·6–4·8]	N.E.	N.E.
FSH (mIU/ml)	0·7 [<0·1–5·4]	4·2 [0·3–18·4]	17·6 [0·3–18·4]
After GnRH-stimulation**	12·0 [10·7–38·1]	N.E.	N.E.
Testosterone (ng/ml)	–	4·3 [1·7–8·7]	3·7 [1·7–8·7]
Calcium metabolism			
Examined age (year)	8·5	16·5	15·0
Calcium (mg/dl)	9·7 [8·8–10·5]	9·2 [8·9–10·6]	9·8 [8·9–10·6]
Inorganic phosphate (mg/dl)	3·9 [3·7–5·6]	4·6 [3·1–5·0]	3·8 [3·2–5·1]
Alkaline phosphatase (IU/l)	458 [343–917]	623 [225–680]	309 [225–680]
Intact PTH (pg/ml)	23 [10–65]	43 [10–65]	28 [10–65]
PTHrP (pmol/l)	N.E.	<1·1 [<1·1]	N.E.

(continued)

Table 1. (continued)

	Case 1*	Case 2	Case 3
$1,25(OH)_2$ vitamin D (pg/ml)	50 [13–79]	67 [13–79]	50 [13–79]
Urine calcium/creatinine ratio (mg/mg)	0·82 [<0·25]	0·24 [<0·25]	0·44 [<0·25]
%TRP	92 [80–96]	95 [80–96]	94 [80–96]
Others	Feeding difficulties	Feeding difficulties Oligohydramnios	

SDS, standard deviation score; OFC, occipitofrontal circumference; BMI, body mass index; MRI, magnetic resonance imaging; CT, computed tomography; ACTH, adrenocorticotropic hormone; R, right; L, left; LH, luteinizing hormone; FSH, follicle-stimulating hormone; GnRH, gonadotropin-releasing hormone; PTH, parathyroid hormone; PTHrP, PTH-related protein; TRP, tubular reabsorption of phosphate; N.E., not examined; and B, bilateral.
Biochemical values indicate basal blood values, except for those specifically defined.
Birth and present length/height, weight, OFC and BMI have been assessed by sex- and gestational- or age-matched Japanese reference data reported in the literature[26,27] and in the Ministry of Health, Labor, and Welfare Database (http://www.e-stat.go.jp/SG1/estat/GL02020101.do).
The values in brackets represent age- and sex-matched reference values in Japanese children.[28]
The conversion factor to the SI unit: 0·220 for ACTH (pmol/l), 27·6 for cortisol (nmol/l), 0·028 for aldosterone (nmol/l), 3·46 for testosterone (nmol/l), 0·25 for calcium (nmol/l), 0·323 for inorganic phosphate (nmol/l), 0·106 for intact PTH (pmol/l), 2·40 for $1,25(OH)_2$ vitamin D (pmol/l) and 1·0 for plasma renin activity (μg/l/h), active renin concentration (ng/l), Na (nmol/l), K (nmol/l), Cl (nmol/l), LH (IU/l), FSH (IU/l), alkaline phosphatase (IU/l) and PTHrP (pmol/l).
*Clinical findings before 3 years of age have been reported previously.[7]
†ACTH 0·25 mg bolus i.v.; blood sampling at 60 min.
‡Electrolyte values at the time of severe gastroenteritis; other biochemical data in reference to adrenal dysfunction were obtained after recovery from gastroenteritis and before glucocorticoid supplementation therapy.
§Reference age for Tanner stage 2 breast development in Japanese girls.[29]
¶Reference age for Tanner stage 4 pubic hair development in Japanese boys.[29]
**GnRH 100 $\mu g/m^2$ bolus i.v.; blood sampling at 0, 30, 60, 90, and 120 min.

Table 2. Summary of clinical features of cases 1–3

	Case 1	Case 2	Case 3
CDKN1C mutation	Yes	Yes	No
Previously reported IMAGe syndrome-compatible phenotype			
IUGR	Yes	Yes	Yes
Metaphyseal dysplasia	Yes	Yes	Yes
Adrenal hypoplasia	Yes*	Yes*	Yes*
Genital abnormality	(Female)	Yes	Yes
Hypercalciura†	Yes	No	Yes
Hitherto undescribed findings			
Body habitus	Relative macrocephaly	Relative macrocephaly	Relative macrocephaly
Skeletal			Arachnodactyly Lack of slender bones
Adrenal		FGD-like phenotype with no obvious mineralocorticoid deficiency	
Genital	Apparently normal pituitary-gonadal endocrine function	Apparently normal pituitary-gonadal endocrine function	Apparently normal pituitary-gonadal endocrine function
Others	Feeding difficulties	Feeding difficulties Oligohydramnios	

IUGR, intrauterine growth retardation; and FGD, familial glucocorticoid deficiency.
*Undetectable on magnetic resonance imaging and/or computed tomography.
†Frequent but not invariable feature.

pre- and postnatal body growth was severely impaired, pre- and postnatal OFC was relatively well preserved. In this regard, while *CDKN1C* is preferentially expressed from the maternal allele in most tissues, it is biparentally expressed at least in the foetal brain.[10] This expression pattern would be relevant to the relative macrocephaly in IMAGe syndrome. Notably, the combination of severely compromised body growth and well-preserved OFC is also characteristic of Silver–Russell syndrome (SRS) resulting

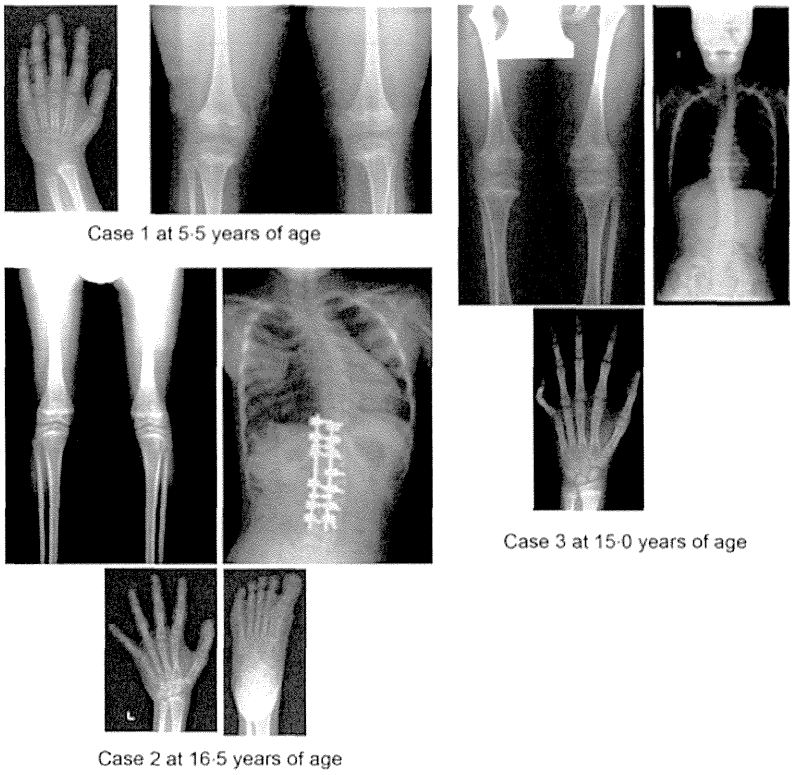

Fig. 2 Representative skeletal roentgenograms in cases 1–3.

from *H19*-DMR hypomethylation (epimutation),[11] and this is primarily consistent with paternal expression of the growth-promoting gene *IGF2* in the body and biparental expression of *IGF2* in the brain.[12] Thus, loss-of-imprinting in the brain tissue appears to underlie relative macrocephaly in both IMAGe syndrome and SRS.

Second, skeletal abnormalities including metaphyseal dysplasia were identified in cases 1 and 2. In this regard, skeletal phenotype of mice lacking *Cdkn1c* is grossly opposite of parathyroid hormone-related protein (PTHrP)-null phenotype,[13,14] and PTHrP permits skeletal development at least in part by suppressing *Cdkn1c* expression.[15] Thus, while serum calcium and calcium homeostasis-related factors were normal in cases 1 and 2, dysregulated PTHrP and/or PTH/PTHrP receptor signalling might be relevant to skeletal abnormalities in patients with gain-of-function mutations of *CDKN1C*. In addition, such a possible signalling defect might also be relevant to the frequent occurrence of hypercalciuria in IMAGe syndrome.

Third, adrenal dysfunction was mild in case 2, while case 1 experienced adrenal crisis in infancy as previously reported in patients with *CDKN1C* mutations.[1,3,4] Indeed, adrenal phenotype of case 2 is similar to that of patients with FGD rather than adrenal hypoplasia.[8,9] Our results therefore would expand the clinical spectrum of adrenal dysfunction in patients with *CDKN1C* mutations. For adrenal dysfunction, cortisol and aldosterone values remained within the normal range at the time of adrenal crisis in case 1 (Table 1). However, as adrenocorticotropic hormone and active renin concentrations were markedly increased, the overall results would be consistent with primary hypoadrenalism, as has been described previously.[16] This notion would also apply to the adrenal dysfunction in case 3 who had apparently normal aldosterone value and markedly increased plasma renin activity at the time of adrenal crisis.

Lastly, although male case 2 had bilateral cryptorchidism and small testes, pituitary-gonadal endocrine function was apparently normal as was secondary sexual development. Previously reported patients with *CDKN1C* mutations, as well as those who have not been examined for *CDKN1C* mutations, also have undermasculinized external genitalia in the presence of apparently normal endocrine function and pubertal development.[1–4,17,18] Notably, an episode of oligohydramnios was found in case 2 and has also been described in a 46,XY IMAGe syndrome patient with cryptorchidism.[19] This may imply the presence of placental hypoplasia and resultant chorionic gonadotropin deficiency as an underlying factor for genital anomalies.[11] In support of this notion, imprinted genes are known to play a pivotal role in body and placental growth,[20] and SRS is often associated with oligohydramnios, placental hypoplasia and undermasculinization.[11,21]

Genetic heterogeneity in IMAGe syndrome

Molecular data in case 3 imply the presence of genetic heterogeneity in IMAGe syndrome. Indeed, there was neither demonstrable *CDKN1C* mutation nor evidence for increased *CDKN1C* expression, while a pathologic mutation leading to gain-of-function or

increased expression of *CDKN1C* might reside on an unexamined region(s) such as promoter or enhancer sequences. In this regard, while case 3 showed IMAGe syndrome-compatible clinical features such as IUGR, metaphyseal dysplasia, adrenal hypoplasia and genital abnormalities, case 3 lacked slender bones and had arachnodactyly, in contrast to *CDKN1C*-mutation-positive cases 1 and 2. Such mild but discernible phenotypic variation might reflect the genetic heterogeneity. This matter might be clarified in the future by extensive studies such as exome or whole-genome sequencing. In particular, when such *CDKN1C*-mutation-negative patients with IMAGe syndrome-compatible phenotype have been accumulated, a novel gene(s) mutated in such patients may be identified. In this regard, if such a gene(s) exist, it is predicted to reside in the signal transduction pathway involving *CDKN1C*.

Relevance of CDKN1C mutations to atypical IMAGe syndrome and SRS

CDKN1C mutations have also been identified in atypical IMAGe syndrome and SRS (Fig. 1a). Hamajima *et al.* revealed a maternally inherited p.Ile272Ser mutation in three siblings (two males and one female) who manifested IUGR and adrenal insufficiency, and male genital abnormalities, but had no skeletal lesion.[22] Similarly, Brioude *et al.* found a maternally transmitted p.Arg279Leu mutation in six relatives (all females) from a four-generation family who satisfied the SRS diagnostic criteria,[23,24] after studying 97 SRS patients without known causes of SRS, that is, hypomethylation (epimutation) of the *H19*-DMR, duplication of the ICR2 and maternal uniparental disomy for chromosome 7 (upd(7)mat).[24] Notably, although both mutations had no significant effect on a cell cycle, they were associated with increased protein stability that appears to be consistent with the gain-of-function effects.[22,24] Such increased stability was also found for IMAGe-associated missense mutant proteins,[22] and an altered cell cycle with a significantly higher proportion of cells in the G1 phase was shown for an IMAGe-associated p.Arg279Pro mutation.[24] It is possible therefore that relatively severe *CDKN1C* gain-of-function effects lead to IMAGe syndrome and relatively mild *CDKN1C* gain-of-function effects result in SRS, with intermediate *CDKN1C* gain-of-function effects being associated with atypical IMAGe syndrome.[24]

Thus, it would not be surprising that cases 1–3 also met the SRS diagnostic criteria (Table 3).[23,24] Indeed, cases 1–3, as well as *CDKN1C*-mutation-positive SRS patients,[24] exhibited pre- and post-natal growth failure with relative macrocephaly and frequently manifested feeding difficulties and/or low body mass index (BMI) at two years of age. However, while relative macrocephaly is usually obvious at birth in SRS patients with *H19*-DMR epimutations and upd(7)mat,[21,23,25] it is more obvious at 2 years of age than at birth in *CDKN1C*-mutation-positive SRS patients.[24] Furthermore, *CDKN1C*-mutation-positive SRS patients are free from body asymmetry,[24] as are typical and atypical IMAGe syndrome patients described in this study and in the previous studies.[1–4,7,22] Thus, SRS caused by *CDKN1C* mutations may be characterized by clinically discernible macrocephaly at two years of age and lack of body asymmetry.

Table 3. Silver–Russell syndrome phenotypes in cases 1–3 and in affected relatives reported by Brioude *et al.*

	Case 1	Case 2	Case 3	Brioude *et al.**
Mandatory criteria				
IUGR†	Yes	Yes	Yes	4/4
Scoring system criteria				
Postnatal short stature (≤−2 SDS)	Yes	Yes	Yes	4/4
Relative macrocephaly‡	Yes	Yes	Yes	4/4§
Prominent forehead during early childhood	Yes	Yes	Yes	4/4
Body asymmetry	No	No	No	0/4
Feeding difficulties during early childhood and/or low BMI (<−2·0 SDS) around 2 years of age	Yes	Yes	Unknown	3/4 (1/4 & 2/4)¶

IUGR, Intrauterine growth retardation; SDS, standard deviation score; and BMI, body mass index.
The SRS diagnostic criteria proposed by Netchine *et al.*[23] and Brioude *et al.*[24] (low BMI around 2 years of age is included in Brioude *et al.*, but not in Netchine *et al.*): The diagnosis of SRS is made, when mandatory criteria plus at least three of the five scoring system criteria are observed. For detailed clinical features in cases 1–3, see Table 1.
*While six relatives were found to have *CDKN1C* mutation, detailed clinical features have been obtained in four mutation-positive relatives.[24]
†Birth length and/or birth weight ≤−2 SDS for gestational age.
‡SDS for birth length or birth weight minus SDS for birth occipitofrontal circumference ≤−1·5.
§Relative macrocephaly is more obvious at 2 years of age (4/4) than at birth (2/4).
¶One patient is positive for feeding difficulties, and other two patients are positive for low BMI.

Conclusion

In summary, we studied three patients with IMAGe syndrome. The results provide implications for phenotypic spectrum, underlying factor(s) in the development of each phenotype and genetic heterogeneity in IMAGe syndrome, as well as a phenotypic overlap between IMAGe syndrome and SRS. Further studies will permit to elucidate such matters.

Funding

This study was supported in part by Grants-in-Aid for Scientific Research (A) (25253023) and for Scientific Research on Innovative Areas (22132004-A01) from the Ministry of Education, Culture, Sports, Science and Technology, by Grant for Research on Intractable Diseases from the Ministry of Health, Labor and Welfare (H24-048), and by Grants from National Center for Child Health and Development (23A-1, 24-7 and 25-10).

Declaration of interest

The authors have nothing to declare.

References

1 Vilain, E., Le Merrer, M., Lecointre, C. *et al.* (1999) IMAGe, a new clinical association of intrauterine growth retardation, metaphyseal dysplasia, adrenal hypoplasia congenita, and genital anomalies. *Journal of Clinical Endocrinology and Metabolism*, **84**, 4335–4340.

2 Balasubramanian, M., Sprigg, A. & Johnson, D.S. (2010) IMAGe syndrome: case report with a previously unreported feature and review of published literature. *American Journal of Medical Genetics A*, **152A**, 3138–3142.

3 Bergadá, I., Del Rey, G., Lapunzina, P. *et al.* (2005) Familial occurrence of the IMAGe association: additional clinical variants and a proposed mode of inheritance. *Journal of Clinical Endocrinology and Metabolism*, **90**, 3186–3190.

4 Arboleda, V.A., Lee, H., Parnaik, R. *et al.* (2012) Mutations in the PCNA-binding domain of CDKN1C cause IMAGe syndrome. *Nature Genetics*, **44**, 788–792.

5 Demars, J. & Gicquel, C. (2012) Epigenetic and genetic disturbance of the imprinted 11p15 region in Beckwith-Wiedemann and Silver-Russell syndromes. *Clinical Genetics*, **81**, 350–361.

6 Lee, M.-H., Reynisdottir, I. & Massague, J. (1995) Cloning of p57(KIP2), a cyclin-dependent kinase inhibitor with unique domain structure and tissue distribution. *Genes and Development*, **9**, 639–649.

7 Amano, N., Naoaki, H., Ishii, T. *et al.* (2008) Radiological evolution in IMAGe association: a case report. *American Journal of Medical Genetics A*, **146A**, 2130–2133.

8 El-Khairi, R., Martinez-Aguayo, A., Ferraz-de-Souza, B. *et al.* (2011) Role of DAX-1 (NR0B1) and steroidogenic factor-1 (NR5A1) in human adrenal function. *Endocrine Development*, **20**, 38–46.

9 Meimaridou, E., Hughes, C.R., Kowalczyk, J. *et al.* (2013) Familial glucocorticoid deficiency: new genes and mechanisms. *Molecular and Cellular Endocrinology*, **371**, 195–200.

10 Matsuoka, S., Thompson, J.S., Edwards, M.C. *et al.* (1996) Imprinting of the gene encoding a human cyclin-dependent kinase inhibitor, p57KIP2, on chromosome 11p15. *Proceedings of the National Academy of Sciences of the USA*, **93**, 3026–3030.

11 Yamazawa, K., Kagami, M., Nagai, T. *et al.* (2008) Molecular and clinical findings and their correlations in Silver-Russell syndrome: implications for a positive role of IGF2 in growth determination and differential imprinting regulation of the IGF2-H19 domain in bodies and placentas. *Journal of Molecular Medicine*, **86**, 1171–1181.

12 Ulaner, G.A., Yang, Y., Hu, J.F. *et al.* (2003) CTCF binding at the insulin-like growth factor-II (IGF2)/H19 imprinting control region is insufficient to regulate IGF2/H19 expression in human tissues. *Endocrinology*, **144**, 4420–4426.

13 Zhang, P., Leigeois, N.J., Wong, C. *et al.* (1997) Altered cell differentiation and proliferation in mice lacking p57(KIP2) indicates a role in Beckwith-Wiedemann syndrome. *Nature*, **387**, 151–158.

14 Karaplis, A.C., Luz, A., Glowacki, J. *et al.* (1994) Lethal skeletal dysplasia from targeted disruption of the parathyroid hormone-related peptide gene. *Genes & Development*, **8**, 277–289.

15 MacLean, H.E., Guo, J., Knight, M.C. *et al.* (2004) The cyclin-dependent kinase inhibitor p57(Kip2) mediates proliferative actions of PTHrP in chondrocytes. *Journal of Clinical Investigation*, **113**, 1334–1343.

16 Stewart, P.M. & Krone, N.P. (2011) The adrenal cortex. In: S. Melmed, K.S. Polonsky, P.R. Larsen, H.N. Kronenberg eds. Williams Textbook of Endocrinology, 12th edn. Elsevier, Saunders, 479–577.

17 Lienhardt, A., Mas, J.C., Kalifa, G. *et al.* (2002) IMAGe association: additional clinical features and evidence for recessive autosomal inheritance. *Hormone Research*, **57**(Suppl 2), 71–78.

18 Pedreira, C.C., Savarirayan, R. & Zacharin, M.R. (2004) IMAGe syndrome: a complex disorder affecting growth, adrenal and gonadal function, and skeletal development. *Journal of Pediatrics*, **144**, 274–277.

19 Ko, J.M., Lee, J.H., Kim, G.H. *et al.* (2007) A case of a Korean newborn with IMAGe association presenting with hyperpigmented skin at birth. *European Journal of Pediatrics*, **166**, 879–880.

20 Fowden, A.L., Sibley, C., Reik, W. *et al.* (2006) Imprinted genes, placental development and fetal growth. *Hormone Research*, **65** (Suppl 3), 50–58.

21 Wakeling, E.L., Amero, S.A., Alders, M. *et al.* (2010) Epigenotype-phenotype correlations in Silver-Russell syndrome. *Journal of Medical Genetics*, **47**, 760–768.

22 Hamajima, N., Johmura, Y., Suzuki, S. *et al.* (2013) Increased protein stability of CDKN1C causes a gain-of-function phenotype in patients with IMAGe syndrome. *PLoS ONE*, **8**, e75137.

23 Netchine, I., Rossignol, S., Dufourg, M.N. *et al.* (2007) 11p15 imprinting center region 1 loss of methylation is a common and specific cause of typical Russell-Silver syndrome: clinical scoring system and epigenetic-phenotypic correlations. *Journal of Clinical Endocrinology and Metabolism*, **92**, 3148–3154.

24 Brioude, F., Oliver-Petit, I., Blaise, A. *et al.* (2013) CDKN1C mutation affecting the PCNA-binding domain as a cause of familial Russell Silver syndrome. *Journal of Medical Genetics*, **50**, 823–830.

25 Fuke, T., Mizuno, S., Nagai, T. *et al.* (2013) Molecular and clinical studies in 138 Japanese patients with Silver-Russell syndrome. *PLoS ONE*, **8**, e60105.

26 Suwa, S., Tachibana, K., Maesaka, H. *et al.* (1992) Longitudinal standards for height and height velocity for Japanese children from birth to maturity. *Clinical Pediatric Endocrinology*, **1**, 5–14.

27 Inokuchi, M., Matsuo, N., Anzo, M. *et al.* (2007) Body mass index reference values (mean and SD) for Japanese children. *Acta Paediatrica*, **96**, 1674–1676.

28 Japan Public Health Association. (1996) Normal Biochemical Values in Japanese Children. Sanko Press, Tokyo, (in Japanese).

29 Matsuo, N. (1993) Skeletal and sexual maturation in Japanese children. *Clinical Pediatric Endocrinology*, **2**(Suppl), 1–4.

Supporting Information

Additional Supporting Information may be found in the online version of this article:

Table S1. Primers utilized in this study.

SCIENTIFIC REPORTS

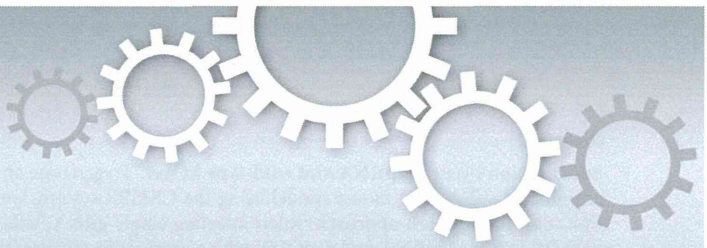

OPEN

SUBJECT AREAS:
GENETIC ENGINEERING
CARTILAGE

Received
21 February 2014

Accepted
3 June 2014

Published
23 June 2014

Correspondence and requests for materials should be addressed to M.I. (inui-m@ncchd.go.jp) or S.T. (takada-s@ncchd.go.jp)

Rapid generation of mouse models with defined point mutations by the CRISPR/Cas9 system

Masafumi Inui[1], Mami Miyado[2], Maki Igarashi[2], Moe Tamano[1], Atsushi Kubo[3], Satoshi Yamashita[1], Hiroshi Asahara[1,3,4,5], Maki Fukami[2] & Shuji Takada[1]

[1]Department of Systems BioMedicine, National Research Institute for Child Health and Development, Tokyo 157-8535, Japan, [2]Department of Molecular Endocrinology, National Research Institute for Child Health and Development, Tokyo 157-8535, Japan, [3]Department of Systems BioMedicine, Graduate School of Medical and Dental Sciences, Tokyo Medical and Dental University, Tokyo 113-8510, Japan, [4]CREST, Japan Science and Technology Agency (JST), Saitama 332-0011, Japan, [5]Department of Molecular and Experimental Medicine, The Scripps Research Institute, 10550 N. Torrey Pines Rd., La Jolla, CA 92037, USA.

Introducing a point mutation is a fundamental method used to demonstrate the roles of particular nucleotides or amino acids in the genetic elements or proteins, and is widely used in *in vitro* experiments based on cultured cells and exogenously provided DNA. However, the *in vivo* application of this approach by modifying genomic loci is uncommon, partly due to its technical and temporal demands. This leaves many *in vitro* findings un-validated under *in vivo* conditions. We herein applied the CRISPR/Cas9 system to generate mice with point mutations in their genomes, which led to single amino acid substitutions in proteins of interest. By microinjecting gRNA, hCas9 mRNA and single-stranded donor oligonucleotides (ssODN) into mouse zygotes, we introduced defined genomic modifications in their genome with a low cost and in a short time. Both single gRNA/WT hCas9 and double nicking set-ups were effective. We also found that the distance between the modification site and gRNA target site was a significant parameter affecting the efficiency of the substitution. We believe that this is a powerful technique that can be used to examine the relevance of *in vitro* findings, as well as the mutations found in patients with genetic disorders, in an *in vivo* system.

Introducing point mutations is a widely used experimental approach to evaluate the roles of specific nucleotides or amino acids in the function of the genetic elements or in proteins of interest. Using this technique, various nucleotides and amino acids have been proved to be indispensable for promoter or enhancer activity, as well as for the function or regulation of enzymes, transcription factors and signaling molecules. However, these findings were achieved mainly by *in vitro* experiments using exogenously provided DNA, such as plasmids or virus vectors, and the *in vivo* introduction of defined point mutations at endogenous genomic loci has been uncommon, largely because of the technical and temporal costs associated with such techniques. Thus, the *in vivo* context or relevance of *in vitro* findings has remained unexplored in many cases.

The CRISPR/Cas9 (clustered regularly interspaced short palindromic repeat/CRISPR-associated 9) system is a recently developed genome-engineering tool based on the bacterial CRISPR immune system, in which guide RNA (gRNA) recruits the Cas9 nuclease to the target locus in the genome by sequence complementarity, and induces double strand breaks (DSBs)[1,2]. These DSBs cause small insertions or deletions (indels) following non-homologous end-joining (NHEJ) repair, or can be utilized to introduce defined sequence modifications through a homology-dependent repair (HDR) mechanism[1,2]. While the use of HDR-dependent genomic engineering has been reported in *in vitro* cell culture systems, whether this could be applied in *in vivo* systems to introduce defined point mutations and what parameters affect its efficiency were less explored.

In the present study, we applied the CRISPR/Cas9 system to create a single amino acid substituted mouse model. By microinjecting synthesized RNAs and single-strand oligodeoxynucleotide (ssODN) donor sequences into mouse zygotes, we were able to introduce defined point mutations in the mouse genome, which led to single amino acid substitutions in the proteins of interest, within as short as one to two months. Using this technique, we can now evaluate the *in vivo* relevance of particular nucleotides/amino acids with a low cost and within a short time, which facilitates the elucidation of the *in vivo* context of the findings in cultured cell systems, as well as the *in vivo* screening for the relevant mutation among those found in human patients with various diseases.

Results

Substitution by single gRNA and wild-type hCas9. To generate an amino acid substituted mouse model using the CRISPR system, we first took the simplest approach: microinjecting single gRNA, wild type (WT) hCas9 mRNA and a ssODN with a single base mismatch to the genomic sequence, which caused single amino acid conversion, into mouse zygotes. As a target, a c.274C>T mutation of the *Steroidogenic Factor 1* gene (*Sf-1*, also known as *Ad4BP* or *Nr5a1*)[3], which causes a p.R92W amino acid substitution in the SF-1 protein, was chosen, and gRNAs and ssODNs were designed as shown in Figure 1A.

To examine whether the sequence or location of the gRNAs could affect the efficiency of the substitution, we designed three independent gRNAs (Sf-1gRNA1, 2 and 3), which had their Protospacer-Adjacent Motif (PAM) sequence 52 or 7 bases upstream, or 12 bases downstream, of the target point mutation (Fig. 1A). Three independent ssODNs were also designed, placing the mismatched nucleotide or PAM sequence of gRNA1 and gRNA2 in their center, respectively (Fig. 1A).

Various combinations of gRNAs and ssODNs (Table 1) were mixed with hCas9 mRNA and microinjected into pronuclear stage embryos. The injected zygotes were transferred to pseudo-pregnant females at the two-cell stage, and the obtained pups were examined for the sequence around the *Sf-1* locus. As shown in Table 1, we found total 26 mice with the C>T substitution generated from three out of four experiments (experiments 2, 3 and 4), and 7 of them had biallelic substitutions (Fig. 1B and Table 1). These results show that microinjecting gRNA, WT hCas9 mRNA and the ssODN donor into mouse zygotes is sufficient to introduce a defined single base substitution in their genome.

Of note, while the frequencies of DSB caused by hCas9/gRNAs, which are indicated by the frequencies of mutated alleles, are comparable among 4 experiments (68–89%, $P = 0.75$) (Table 1), the frequencies of designated substitutions vary significantly (0–29.6%, $P < 0.01$) (Table 1). This lack of a correlation between the frequency of the mutation and the substitution to occur suggests that there may be an optimal rate of DSB occurance to introduce HDR-dependent sequence incorporation (such like too frequent DSB might be unfavorable for HDR), or that the distance and/or the mutual position between the substitution target site and gRNA PAM sequences (surrogate DSB point) could affect the substitution efficiency. Our subsequent experiments support the latter possibility (see below). To explore the effect of mutual position between substitution target site and DSB point on substitution efficiency, we designed two additional ssODNs which have similar sequence to ssODN1, but carry point mutations in 36 base upstream or 12 base downstream to the PAM sequence of Sf-1 gRNA3 (Supplementary Fig. S1). ssODNs were microinjected into mouse zygotes with hCas9 mRNA and Sf-1 gRNA3, and the frequency of the designated substitution and the mutated allele in those mice were compared to experiment 4 (Supplementary Table S1). As a result, while 80–95% of mice had mutated alleles in all three experiments, the frequency of the substituted alleles differs substantially: 29.6% with ssODN3, 20.0% with ssODN4, and 0% with ssODN5 (Supplementary Table S1). These results indicate that the probability of the mutation in donor DNA to be incorporated into the genome declines with the distance between the DSB point and the mutation. In addition, the mutation which is at the downstream (3′ side) of PAM sequence showed slightly lower frequency of substitution than the mutation with the same distance from the PAM sequence but is at the upstream (5′ side). Together, these results show that the mutual location of gRNA target site and substitution target site is an important parameter for the efficient introduction of the designated point mutation.

Although there was an efficient generation of targeted point mutations, we observed that many mice with the C>T substitution also received additional random mutations in the flanking regions (Fig. 1C and Table 1). Moreover, it has previously been reported that single gRNA/WT hCas9 may introduce undesired mutations at the genomic loci with similar sequences to the target site (off-target effect)[4–6], which prompted us to test the double nicking strategy[5] to induce more accurate genome modifications in mouse zygotes.

Substitution using two gRNAs and hCas9 D10A (double nicking). Combining a pair of gRNAs with mutated hCas9 (hCas9 D10A), double nicking cause DSB only at the genomic loci where both of the gRNAs bind at an appropriate distance, thus making it highly specific to the target site[5]. To examine whether this set-up could be used for the HDR-dependent genome editing *in vivo*, we aimed to induce the c.1187A>G mutation of the *Sox9* gene, which results in a p.K396R amino acid substitution in the SOX9 protein. Lysine 396 is an evolutionary-conserved post-translational modification site of the SOX9 protein, but its *in vivo* relevance has not been fully examined[7,8]. We designed two gRNAs with a five-base offset where their PAM sequences are positioned about 40 bases upstream and three bases downstream of the A>G substitution site (Fig. 2A). Two ssODNs were designed with several silent mutations within the recognition sequence of gRNA2 to avoid repetitive digestions. An additional silent mutation to eliminate the *Pvu*II site was also designed to facilitate the genotyping (Fig. 2A). Sox9-ssODN1 causes both silent mutations and c.1187A>G substitution (K-to-R substitution), while Sox9-ssODN2 causes only silent mutations (K-to-K substitution) (Fig. 2A, lower panel). The two gRNAs, hCas9 D10A mRNA and 2 ssODNs were mixed and microinjected into zygotes to generate amino acid substituted mice (by Sox9-ssODN1) and negative control mice (by Sox9-ssODN2) simultaneously.

The obtained pups were genotyped as before, and we found that five pups out of 24 (20.8%) with the designated substitution, two of which had a K-to-R substitution (Fig. 2B) and three of which had a K-to-K substitution (Table 2). A frame shift mutation caused by an indel was observed in only one mouse. Thus, double nicking, together with donor ssODN, can also introduce defined point mutations in mouse zygotes. The frequency of the substitution was lower than that of the single gRNA/WT hCas9 condition shown in previous section, but was sufficient to generate mice with two genotypes in a single microinjection experiment by mixing different donor DNAs. Of note, a *Pvu*II site substitution was never observed in the mice with upstream substitutions (Fig. 2B and data not shown). This, together with the results of the experiment 4–6 with *Sf-1*, suggest that only a part of the sequence of the donor DNA near the DSB site will be incorporated through the CRISPR-mediated HDR pathway. Therefore, it is important to place the gRNA target site close enough to the substitution site to achieve efficient substitution.

SOX9-K396R gRNA2 and WT hCas9 mRNA with ssODNs were also microinjected into zygotes to compare the efficiency with double nicking (Table 2). As shown in Table 2, single gRNA with WT hCas9 resulted in a higher mutation frequency (76.9%) as well as substitution frequency (34.6%), and as in the case of *Sf-1*, biallelic substitution and additional random mutations were also observed (Supplementary Fig. S2 and Table 2).

Finally, we compared the off-target effects under the two conditions. Five putative off-target sites of SOX9-K396R gRNA2 were computationally predicted[6], and the sequences of those sites in gRNA/hCas9-injected mice were analyzed (Fig. 3A). As a result, we did not detect any mutations in the total of 250 loci (five off-target sites in 50 mice) examined (Fig. 3B and Table 3), indicating that both single gRNA with WT hCas9 and double nicking introduced designated genetic modification in highly specific manner. To examine if this high specificity could also be observed with other gRNAs, off-target effect of Sf-1 gRNAs were also analyzed. We focused on the mice which received designated substitution in first 4 experiments (total 26 mice shown in Table 1) and examined total of 121 loci, and did not find any off-target mutation (Supplementary Fig. S3 and

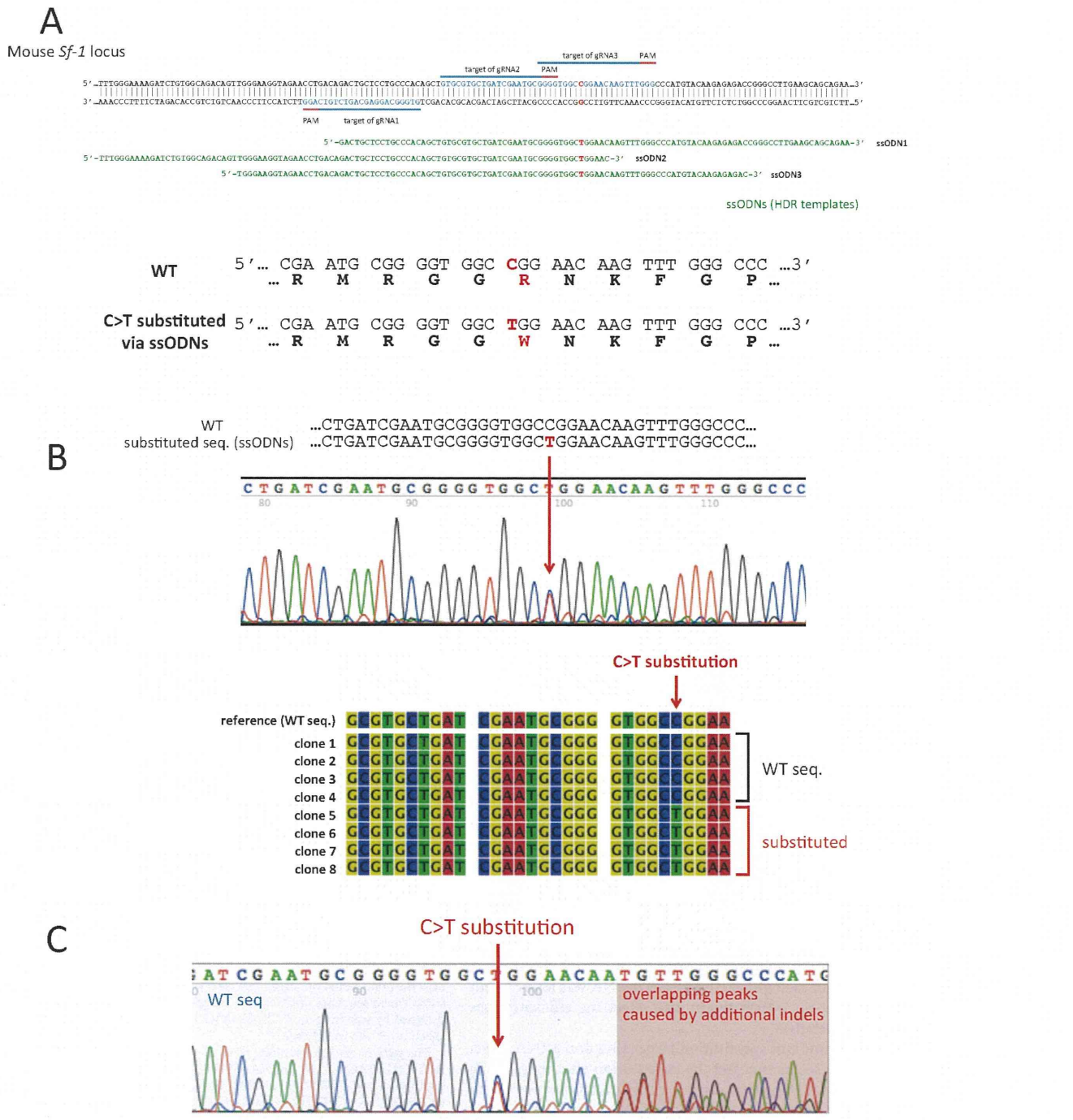

Figure 1 | Introduction of the C>T substitution in *Sf-1* locus. (A) A schematic illustration showing the locations of the gRNAs and ssODNs, along with the mouse *Sf-1* locus. Blue bars and letters indicate the position of the gRNA targets with red bars highlight the PAM sequences. ssODNs are shown in green letters at the corresponding position to the *Sf-1* locus. Red letters indicate the substitution target site in the *Sf-1* locus and corresponding mismatched nucleotides in the ssODNs. The deduced amino acid sequences from wild type (WT) and substituted sequences are shown at the bottom, with red letters indicating the target and the results of the substitution. (B) The results of the sequence analysis of the *Sf-1* locus of a representative mouse, with a monoallelic C>T substitution. The *Sf-1* locus around the gRNA target site was PCR amplified and directly sequenced (Upper panel), or cloned into the plasmid and sequenced independently (Lower panel). The upper panel shows the electropherogram of the direct sequencing results, in which one allele received a C>T substitution. WT and donor DNA sequences are shown on the top, with red letters indicating the mutated nucleotide. The red arrow indicates the overlapping peak caused by the monoallelic substitution. The lower panel shows the sequence alignment of eight independent clones. The eight sequences are separated into two types: the WT sequence and substituted sequences. (C) The results of the direct sequencing of the *Sf-1* locus around the gRNA target site of another representative mouse obtained in experiment 4 shown in Table 1, in which one alleles received C>T substitutions, followed by additional mutation(s) that caused continuous overlapping peaks.

Table 1 | Summary of experiments targeting the *Sf-1* locus

	Microinjection		Survival of zygotes			Result of genotyping				Ratio of genotyping	
Experiment	gRNA	ssODN	2 cell embryo/ injected zygotes	Transferred	Genotyped	Monoallelic substitution (+indel)	Biallelic substitution (+indel)	Indel	WT	Mouse with substituted alleles (%)	Mouse with mutated alleles (%)
1	1	1	128/256	128	39	0 (0)	0 (0)	31	8	0 (0)	31 (79.5)
2	1	2	101/203	101	37	1 (1)	0 (0)	32	4	1 (2.7)	33 (89.2)
3	2	3	124/169	124	51	8 (7)	1 (1)	26	16	9 (17.6)	35 (68.6)
4	3	1	157/217	144	54	10 (7)	6 (5)	28	10	16 (29.6)	44 (81.5)

Supplementary Table S2). Together, these results suggest the ratio of on/off-target mutation is substantially high in this experimental set up.

Discussion

Introducing point mutations is widely used technique in cultured cell based experiments, but uncommon in *in vivo* system partly because of its temporal and technical demands. The standard approach to examine the function of particular nucleotides or amino acids in *in vivo* background has been to create a knock-in or transgenic mouse that carries cDNA or other genetic element with defined point mutation(s). However these techniques require long and laborious procedures such as constructing targeting vectors, cloning of ES cell and/or establishing multiple transgenic mouse lines. Our method overcome those difficulties and possible problems and is ideal to observe the effect of subtle genetic modification under physiological condition.

The CRISPR/Cas9 system has been used to introduce defined genetic modification in cultured cell system[5,9], but whether this could be applied to *in vivo* system and what parameter(s) is influential for its efficiency was less explored. We demonstrated that the CRISPR/Cas9 system, both single gRNA/WT hCas9 and double nicking set-ups, was effective in mouse zygotes with the former having slightly higher efficiency. In our best condition, microinjection of single gRNA with WT hCas9 introduced the point mutation in more than 30% of mice examined, in which 10% of them received biallelic modification, allowing researcher to analyze the mouse model in the founder generation (Note that the possible mosaicism should be considered in analyzing the phenotype of founder generation and we believe that the confirmation in descendant generation is indispensable to conclude genotype-phenotype relationship). We observed higher efficiency with single gRNA with WT hCas9 than double nicking set-up, which is expected because the latter set-up requires two gRNA-hCas9 complexes to be recruited simultaneously to the target site to introduce DSB while one complex is enough for the former. In addition, to inject the same amount of RNAs in total, the concentration of each gRNA and hCas9 mRNA was lower in our double nicking set-up, which might also affect the efficiency (see Methods for the details).

The mutual position of substitution target sites and gRNA target sites (DSB points) seems to affect the substitution efficiency. Using same gRNA and ssODNs with various point mutations, we found that the mutations which are closer to the gRNA target site is incorporated more often than that are farther from DSB point (Supplementary Fig. S1 and Supplementary Table S1). This is in line with the previous report in which the efficiency of gene conversion was examined using plasmid donor DNA and restriction enzyme in cell culture system, and found that the frequency of the substitution declines with the distance from the digestion site[10]. Whether the frequency of substitution varies by using sense (i.e. the same strand of gRNA target) or anti-sense strand sequence for ssODN could be another point to be examined in the future studies.

Surprisingly, we did not observe any off-target effect in our experiments. The total of 371 loci were examined but no indels were detected. This was an unexpected result, since frequent off-target mutagenesis has been reported in human cells[4,5], but is consistent with a rare off-target effect observed in mouse zygotes microinjected with hCas9 and gRNA plasmids[11]. These results do not exclude off-target effects in general, but imply that the cultured cells and mouse zygotes have distinct risks for off-target effects, possibly due to the different stability of the CRISPR/Cas9 components and/or the nuclear/chromatin dynamics between stable cell lines and zygotes under early developmental process. Further accumulation of data is necessary to understand the kinetics of CRISPR mediated genome modification to optimize the experimental parameters for obtaining highest efficiency with minimum off-target effect in various back ground.

In summary, we have established an experimental system to introduce defined point mutations into the mouse genome using the CRISPR/Cas9 system, which enabled us to generate an amino acid substituted mouse model at a low cost and in a short time. The WT hCas9 and double nicking strategy were both effective and the distance between the DSB site and substitution site seems to be an important parameter for determining the substitution efficiency. We believe this technique will be useful to reveal the *in vivo* relevance of particular nucleotides/amino acids identified in *in vitro* systems, as well as to reproduce the genetic variations found in patients of genetic disorders in mouse models.

Methods

Plasmids. hCas9, hCas9 D10A and the gRNA cloning vector[1] were purchased from Addgene (Plasmid ID #41815, #41816 and #41824, respectively). Since the original gRNA cloning vector lacks the partial sequence of the U6 promoter and gRNA scaffold, we first modified it by adding the following sequence: 5′-GTGGAA-AGGACGAAACACCGGCTAGCAGGCCTATCGATGTTTTAGAGCTAGAA-ATAGC-3′ into the *Afl*II site to fill the missing sequence and to facilitate further cloning. gRNA expression vectors were constructed by inverse PCR using this modified vector and the primer pairs shown in the Table below. The PCR products were *Dpn*I digested and used for the transformation of *E. coli* (DH5a). The sequences of the obtained constructs were validated by sequencing.

gRNA design. The gRNAs were designed by searching for "GG" or "CC" sequences near the point mutation target sites, and were defined as N(21)GG or the reverse complement sequence of CCN(21). The gRNA pairs used for double-nicking were designed by searching for CCN(40–48)GG sequences, and the pair closest to the substitution site was chosen.

The gRNAs used in this study were: Sf-1 gRNA1 5′-GTGGGCAGGAGC-AGTCTGTCAGG-3′, Sf-1 gRNA2 5′-GTGCGTGCTGATCGAATGCGGGG-3′, Sf-1 gRNA3 5′-GGGGTGGCCGGAACAAGTTTGGG-3′, SOX9-K396R gRNA1 5′-GCCTGGCTCGCTGCTCAGCGTGG-3′, SOX9-K396R gRNA2 5′-CCAGCGAAC-GCACATCAAGACGG-3′.

RNA synthesis. Template DNAs for *in vitro* transcription were generated by PCR amplification of the ORFs of hCas9 and hCas9 D10A, as well as gRNAs (i.e. guide sequences and scaffold sequences) from each plasmid using PrimeSTAR (TaKaRa) and the primer sequences shown below (the T7 RNA polymerase recognition sequence was attached to the 5′ end of the fw primers). The PCR products were purified and used for the *in vitro* RNA synthesis using mMessage mMachine T7 kit (lifetechnologies). The reaction scale was doubled, and the reaction time was extended to over-night to obtain a sufficient amount of gRNA. The synthesized RNAs were purified using an RNeasy mini kit (Qiagen) with an additional ethanol precipitation.

ssODN. The synthesized single stranded oligonucleotides (110 bases, PAGE purified) were purchased from fasmac.